© 2016. Published by The Company of Biologists Ltd | Journal of Cell Science (2016) 129, 604-620 doi:10.1242/jcs.179325

RESEARCH ARTICLE

WHAMY is a novel actin polymerase promoting myoblast fusion, macrophage cell motility and sensory organ development in *Drosophila*

Klaus Brinkmann[1], Moritz Winterhoff[2], Susanne-Filiz Önel[3], Jörg Schultz[4], Jan Faix[2] and Sven Bogdan[1,*]

ABSTRACT

Wiskott–Aldrich syndrome proteins (WASPs) are nucleation-promoting factors (NPF) that differentially control the Arp2/3 complex. In *Drosophila*, three different family members, SCAR (also known as WAVE), WASP and WASH (also known as CG13176), have been analyzed so far. Here, we characterized WHAMY, the fourth *Drosophila* WASP family member. *whamy* originated from a *wasp* gene duplication and underwent a sub-neofunctionalization. Unlike WASP, we found that WHAMY specifically interacted with activated Rac1 through its two CRIB domains, which were sufficient for targeting WHAMY to lamellipodial and filopodial tips. Biochemical analyses showed that WHAMY promoted exceptionally fast actin filament elongation, although it did not activate the Arp2/3 complex. Loss- and gain-of-function studies revealed an important function of WHAMY in membrane protrusions and cell migration in macrophages. Genetic data further implied synergistic functions between WHAMY and WASP during morphogenesis. Double mutants were late-embryonic lethal and showed severe defects in myoblast fusion. Trans-heterozygous mutant animals showed strongly increased defects in sensory cell fate specification. Thus, WHAMY is a novel actin polymerase with an initial partitioning of ancestral WASP functions in development and subsequent acquisition of a new function in cell motility during evolution.

KEY WORDS: Actin assembly, WASP, JMY, WHAMM, Macrophage, Myoblast fusion, WAVE, Cell migration, Cellular immune response, Sensory organ development

INTRODUCTION

The actin cytoskeleton plays a central role in a number of different cellular functions, such as cell shape changes, cell motility and membrane trafficking. Members of the Wiskott–Aldrich syndrome protein (WASP) family are conserved nucleation-promoting factors (NPF) that activate the Arp2/3 complex, a major actin nucleator in eukaryotic cells (Pollard, 2007; Pollard and Beltzner, 2002; Pollitt and Insall, 2009; Rottner and Stradal, 2011; Takenawa and Suetsugu, 2007). In mammals, the WASP protein family consists of eight different members: the two Wiskott-Aldrich syndrome proteins WASP and N-WASP (also known as WAS and WASL, respectively) (Derry et al., 1994; Miki et al., 1996), the related WASP family Verprolin homologous proteins WAVE1–WAVE3 (also known as SCAR1–SCAR3 and WASF1–WASF3) (Miki et al., 1998), the Wiskott–Aldrich syndrome protein and SCAR homolog WASH (also known as WASH1) (Linardopoulou et al., 2007) and the WHAMM and JMY proteins (Campellone et al., 2008; Zuchero et al., 2009). WASP proteins share a conserved C-terminal Arp2/3-complex-activating WCA module. This module consists of either one or multiple actin-monomer-binding WH2 (W) domains, a central domain (C) and an acidic (A) domain, which mediate Arp2/3 binding (Campellone and Welch, 2010; Stradal and Scita, 2006). Apart from the catalytic WCA module, WASP proteins often share a proline-rich region and a basic region, which bind SH3-domain containing proteins and acidic phosphoinositides, respectively (Suetsugu et al., 2003; Takenawa and Suetsugu, 2007). WASP proteins are regulated by similar molecular principles. Under resting conditions NPFs are primarily inactive and become activated upon binding of the Rho GTPases Cdc42 and Rac1. Additionally, a variety of factors further modulate proper activation and recruitment of WASP proteins (Krause and Gautreau, 2014).

In *Drosophila*, only three WASP subfamily members have been described, namely WAVE, WASP and WASH (also known as CG13176). Insects like *Drosophila* have subsequently lost a WHAMM/JMY gene, although the common ancestor first arose in invertebrates (Kollmar et al., 2012; Veltman and Insall, 2010). Genetic studies indicate that WAVE and WASP are the central activators of the Arp2/3 complex, differentially regulating most aspects of Arp2/3 function in *Drosophila* (Ben-Yaacov et al., 2001; Bogdan et al., 2004, 2005; Bogdan and Klämbt, 2003; Fricke et al., 2009; Leibfried et al., 2008; Stephan et al., 2011; Zallen et al., 2002; Zobel and Bogdan, 2013). These studies highlight distinct, but also overlapping cellular requirements of WAVE and WASP during development. WAVE function is in particular essential for cell shape and morphogenetic cell movements during development (Stephan et al., 2011; Zallen et al., 2002). By contrast, WASP function is needed for cell fate specification of sensory organ precursors (SOPs) and spermatid maturation (Ben-Yaacov et al., 2001; Berger et al., 2008; Mukherjee et al., 2011; Rotkopf et al., 2011). Both, WASP and WAVE are required for myoblast fusion (Abmayr and Pavlath, 2012; Gildor et al., 2009; Berger et al., 2008).

Loss of maternal and zygotic WASP results in late-embryonic lethality due to strong defects in cell fate decisions of neuronal cell lineages and myoblast fusion defects (Ben-Yaacov et al., 2001; Mukherjee et al., 2011; Schafer et al., 2007; Massarwa et al., 2007). Remarkably, animals lacking zygotic WASP function survive until early adulthood (Ben-Yaacov et al.,

[1]Institut für Neurobiologie, Universität Münster, Badestr. 9, Münster 48149, Germany. [2]Institut für Biophysikalische Chemie, Medizinische Hochschule Hannover, Carl-Neuberg Strasse 1, Hannover 30625, Germany. [3]Fachbereich Biologie, Entwicklungsbiologie, Philipps-Universität Marburg, Karl-von-Frisch Str. 8, Marburg 35043, Germany. [4]Center for Computational and Theoretical Biology, Campus Nord and Bioinformatik, Biozentrum, Am Hubland, Universität Würzburg, Würzburg 97074, Germany.

*Author for correspondence (sbogdan@uni-muenster.de)

Received 18 August 2015; Accepted 9 December 2015

Journal of Cell Science

Journal of Cell Science (2016) 129, 604-620 doi:10.1242/jcs.179325

2001). Thus, maternally provided WASP protein is sufficient for proper embryonic and larval development (Ben-Yaacov et al., 2001). Mutant *wasp* flies show no strong morphological defects except a partial loss of sensory bristles. Loss of zygotic Arp2/3 function results in a similar, albeit stronger, neurogenic phenotype suggesting an involvement of additional factors in Arp2/3-dependent SOP development (Rajan et al., 2009). The loss of sensory bristles in *wasp* and *arp2/3* mutants phenocopies *Notch* loss-of-function and is caused by a pIIa-to-pIIb cell fate transformation (Ben-Yaacov et al., 2001). This results in an excess of neurons at the expense of bristle sheath, shaft and socket cells (Ben-Yaacov et al., 2001; Rajan et al., 2009). Recent work further suggests that the WASP–Arp2/3 pathway rather plays an important role in the trafficking of Delta-positive vesicles from the basal area to the apical cortex of the signal-sending pIIb cell (Rajan et al., 2009).

Remarkably, rescue experiments have implied that established activators of WASP, such as Cdc42 or phosphatidylinositol 4,5-bisphosphate (PIP_2), are not required for WASP function, neither for the myoblast fusion process nor for SOP development (Ben-Yaacov et al., 2001). The identity of an independent activator that might act cooperatively to control Arp2/3 function in these contexts is unknown. Here, we present a functional analysis of WHAMY, a new WASP-like protein that regulates cell motility of *Drosophila* blood cells but also synergizes with WASP during embryonic muscle formation and cell fate specification of adult SOPs.

RESULTS

WHAMY originates from a duplication of the *wasp* gene

Sequence analysis revealed that WHAMY is a paralog of WASP, which arose from duplication in the genus *Drosophila*. WASP and WHAMY carry two WH2 domains in their C-terminus (Fig. 1A). Although WASP contains one CRIB domain (amino acids 230–293) and an N-terminal WH1 domain (amino acids 31–140), WHAMY has two N-terminal CRIB domains (amino acids 4–70 and 185–254; Fig. 1A). As the domain architecture of WASP is conserved throughout the eukaryotes, this indicates a loss of the WH1 domain in WHAMY followed by an accretion of a CRIB domain. To unravel the origin of this domain, a phylogenetic tree of CRIB domains of both proteins from different *Drosophila* species and, as an outgroup, *Anopheles gambiae* and *Culex quinquefasciatus*, was calculated (Fig. 1B; alignment in Table S1). Here, the *Drosophila* WASP CRIB domains were the clear outgroup to both WHAMY domains. Thus, an internal duplication is the origin of the second CRIB domain in WHAMY.

Gene duplication frequently leads to a phase of relaxed selection (Lynch and Conery, 2000). This can be followed by neofunctionalization, indicated by a phase of positive selection. In addition, in the case of the CRIB duplication, models allowing for a different (faster) evolution rate after duplication fitted the data significantly ($P<0.01$) better than those assuming a single rate over the whole tree (Yang, 2007). More detailed models assuming an increased rate after duplication of WASP and duplication of the CRIB domains fitted the data as good as models assuming an increased rate over the whole WHAMY subtree (Fig. S1). This increased rate in WHAMY compared to WASP was also found when analysing the region C-terminal to the CRIB domains independently (Table S2). Thus, the duplication of the whole gene had a comparable effect on the WHAMY CRIB domains to that of their succeeding duplication. This could indicate that the neofunctionalization of the CRIB domains is still in progress. Still, even considering site-specific models, no substantial traces of a phase of positive selection were detected (Yang, 1998). A multiple sequence alignment of WASP and WHAMY CRIB domains allowed for the identification of sites that might be involved in a change of function (Fig. 1C; Table S1). Most interestingly, there were sites that showed a different conservation between WASP and WHAMY. These differences affected one or both WHAMY CRIB domains. Mapping these sites onto the structure of a WASP CRIB domain (PDB ID 1CEE) together with the ligand shows that these sites are in positions responsible for the specificity of ligand binding (Abdul-Manan et al., 1999; Fig. 1C). These sites might therefore be involved in a change of substrate specificity for the CRIB domains in WHAMY.

WHAMY binds activated Rac1 and localizes at lamellipodial tips of S2R+ cells in a manner depending on both CRIB domains

Based on the above prediction, we first tested whether the two CRIB domains of WHAMY are functional binding sites for active Cdc42 or Rac1. We performed pulldown experiments using either GST–Cdc42 or GST–Rac1 incubated with lysates prepared from S2R+ cells expressing different WHAMY–EGFP fusions lacking either one or both CRIB domains. Full-length WHAMY–EGFP strongly bound Cdc42, but this binding was, however, independent of the nucleotide-binding status of Cdc42 (Fig. 1D). The truncated WHAMY proteins lacking either the first (ΔCRIB1) or the second CRIB domain (ΔCRIB2) still bound Cdc42-GDP. However, both CRIB domains differed in their capacity to bind to activated Cdc42. Only the deletion of the second CRIB domain led to loss of binding. Thus, the differences observed in the sequence between the two CRIB domains indeed result in functional divergence. Notably, WHAMY interacted specifically with GTP-loaded Rac1. Pulldown experiments with ΔCRIB1 or ΔCRIB2 deletions further indicated that, in contrast to with Cdc42, both CRIB domains of WHAMY were equally required for the interaction with activated Rac1. Again, loss of both CRIB domains entirely abolished Rac1 binding (Fig. 1D). Therefore, we conclude that, unlike WASP, WHAMY is not an effector of Cdc42 but rather acts downstream of Rac1.

We next examined the subcellular localization of WHAMY–EGFP in transfected S2R+ cells. WHAMY–EGFP strongly localized at the leading edge and at dynamic vesicles (Fig. 1E,E′; Movie 1). Interestingly, deletion of both CRIB domains prevented WHAMY targeting to lamellipodial tips, whereas the vesicular localization was not affected (Fig. 1F,F′; Movie 2). Thus, we conclude that Rac1 binding mediates the localization of WHAMY to lamellipodial tips.

Structured illumination microscopy (SIM) further revealed that WHAMY-marked vesicles overlapped with F-actin, suggesting that the vesicles move at the tips of actin tails (Fig. 1G; see also Movies 1 and 2). Co-transfection experiments with different Rab–Cherry fusions indicated that a large majority of the vesicles marked by WHAMY–EGFP were Rab11-positive recycling endosomes (mean Pearson coefficient, 0.67; Fig. 1H,I; Movie 3).

WHAMY promotes the assembly of linear actin filaments

The prominent localization of WHAMY at the leading edge prompted us to analyze the activity of WHAMY in regulating actin assembly *in vitro*. Recombinant full-length WHAMY (WHAMY-FL) was sufficient to stimulate actin polymerization in a concentration-dependent manner, albeit with markedly slower kinetics as compared to the C-terminal half of the *Drosophila* formin Diaphanous (Dia; Fig. 2A). Thus, we reasoned that

Journal of Cell Science (2016) 129, 604-620 doi:10.1242/jcs.179325

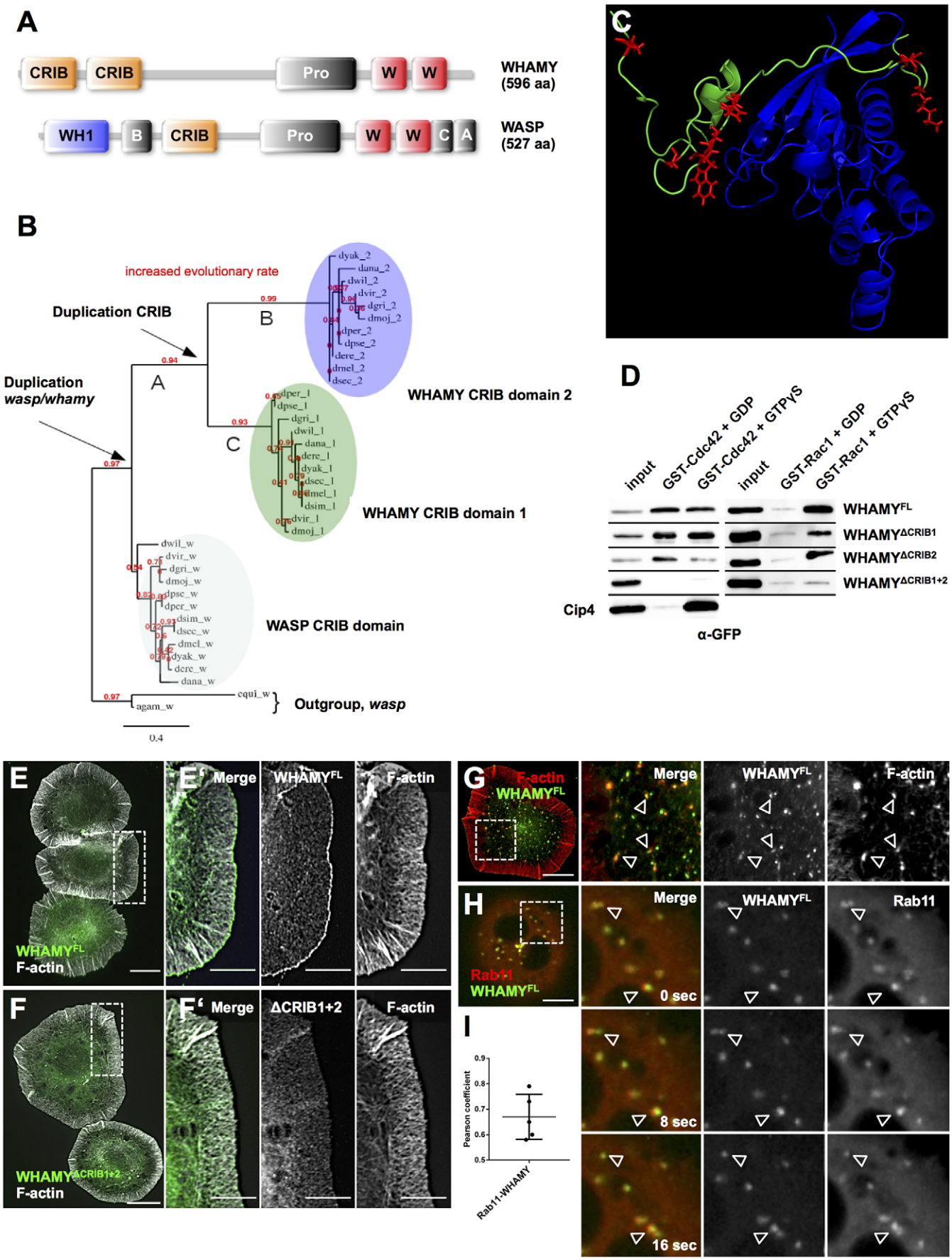

Fig. 1. See next page for legend.

Journal of Cell Science

Journal of Cell Science (2016) 129, 604-620 doi:10.1242/jcs.179325

Fig. 1. WHAMY originates from a *wasp* gene duplication. (A) Similar modular domain organization of *Drosophila* WHAMY and WASP. WH1, WASP homology 1 domain; B, a stretch of basic amino acids; CRIB, Cdc42/Rac-interactive binding domain; Pro, proline-rich region; W, WH2; C, central domain; A, acidic domain. (B) Phylogenetic tree of selected dipteran WASP and WHAMY CRIB domains. Estimates of the approximate likelihood ratio tests in red. (C) Structure of the WASP CRIB domain (green, PDB ID 1CEE). Ligand is shown in blue. Residue changes in the first CRIB domain of WHAMY are indicated in red. (D) GST–Cdc42 and GST–Rac1 pulldown experiments with lysates of S2R+ cells transfected with full-length WHAMY–EGFP (WHAMY-FL), or different truncated WHAMY–EGFP fusions lacking either both or single CRIB domains. The *Drosophila* Cdc42-interacting protein 4 (Cip4) serves as a positive control because it specifically interacts with Cdc42 loaded with GTPγS as previously described (Fricke et al., 2009). (E,E′,F,F′) Structured illumination microscopy (SIM) images of *Drosophila* S2R+ cells transfected with (E,E′) full-length WHAMY–EGFP and (F,F′) with WHAMY–EGFP lacking both CRIB domains (ΔCRIB1+2). E and F show entire SIM images; the white boxes highlight the area of magnified images shown in E′ and F′. Cells were co-stained with phalloidin (white, F-actin). (G) SIM image of a WHAMY–EGFP-transfected cell (green) co-stained for F-actin (red); the white box highlights the area of the magnified images. Arrowheads mark positions of WHAMY-positive vesicles colocalizing with F-actin. (H) Frames from a spinning disk microscopy time-lapse movie (Movie 3) of an S2R+ cell co-expressing WHAMY–EGFP and Rab11–Cherry. Arrowheads indicate positions of colocalization between WHAMY and Rab11 at vesicles. (I) Colocalization analysis of WHAMY and Rab11 at vesicles based on Pearson's colocalization coefficient (n=5 cells). Bar represents mean±s.d. Scale bars: 10 µm (E,F); 5 µm (E′,F′,G,H).

WHAMY-FL might be autoinhibited and require interaction with the small GTPase Rac1 to display full activity. Of note, in pulldown experiments active GST–Cdc42 showed stronger interaction with WHAMY-FL as compared to active GST–Rac1 (Fig. S2A). However, given that the Cdc42–WHAMY interaction was unspecific (Fig. 1D), we continued the *in vitro* analysis on WHAMY-FL with constitutively active Rac1-V12. Increasing concentrations of Rac1 further stimulated WHAMY-FL-mediated actin polymerization, indicative of WHAMY activation by this GTPase (Fig. 2B).

Given that other members of the *Drosophila* WASP protein family act as NPFs for the Arp2/3 complex, we next tested whether WHAMY additionally exhibits NPF activity towards the Arp2/3 complex. However, and even in the presence of active Rac1, WHAMY-FL did not activate the Arp2/3 complex (Fig. 2C). By contrast, Cdc42-activated WASP promoted Arp2/3-complex-mediated actin assembly even at low nanomolar concentrations (Fig. 2C). To explore the potential synergy between WHAMY and WASP observed during morphogenesis (see below), we performed GST pulldown assays with recombinant GST–WASP and WHAMY-FL alone and in presence of constitutively active Cdc42 and Rac1. Indeed, a substantial fraction of recombinant WHAMY-FL was pulled down by GST–WASP-coated beads but not by the control beads coated with GST alone (Fig. 2D). Surprisingly, the WHAMY–WASP interaction was not further strengthened by addition of Cdc42 or Rac1. Control experiments without WASP confirmed that activated Cdc42 and activated Rac1 alone did not affect the amount of WHAMY pulled down with GST-coated beads (Fig. S4B).

Up to an equimolar ratio, WHAMY-FL-mediated actin polymerization was stimulated by increasing concentrations of Cdc42-activated WASP, and this effect was augmented even more by active Rac1 (Fig. 2E). Addition of WASP at concentrations above 200 nM, however, resulted in decreased actin polymerization rates and lower plateau values indicative of actin monomer sequestration by WASP WH2 domains. Next, we assayed Arp2/3 complex activation by WASP in the presence of WHAMY-FL. Although WHAMY-FL did not directly stimulate the ability of WASP to activate the Arp2/3 complex, it enhanced the Arp2/3-complex-dependent actin polymerization mediated by Cdc42-activated WASP (Fig. 2F). Consistent with previous studies, we also found that full-length WASP alone was not entirely autoinhibited with regard to Arp2/3 complex activation (Fricke et al., 2009; Rohatgi et al., 1999). Given the observed WHAMY–WASP interaction, these findings therefore suggest that WHAMY might generate mother filaments in close vicinity of the Arp2/3 complex to promote Arp2/3-complex-dependent actin assembly.

WHAMY exhibits moderate nucleation but profound filament elongation activities

To gain deeper insights into the activities of WHAMY, we performed single-filament total internal reflection fluorescence (TIRF) microscopy assays. In the presence of 100 nM WHAMY-FL, about three times more filaments were formed as compared to the actin control, indicating moderate nucleation activity of WHAMY-FL (Fig. 3A,B). Notably, WHAMY formed bright actin-rich clusters at the sides or the ends of the filaments that were capable of nucleating new actin filaments in the absence of profilin (Movie 4). Intriguingly, upon binding of free filament barbed ends to WHAMY clusters, these filaments were rapidly elongated in short bursts with up to >200 subunits/s demonstrating exceptional actin polymerase activity (Fig. 3C–E; Movie 4). In the presence of 5 µM profilin, the nucleation activity of WHAMY was almost abolished and the filament elongation rate diminished to ∼90 subunits/s. Interestingly, the WHAMY clusters as well as WHAMY-elongated filaments appeared much brighter in these conditions (Fig. 3D; Movie 4). Given that profilin exhibits low affinity to Cys^{374}-labeled actin (Kovar et al., 2006), these data indicate that WHAMY cannot efficiently bind to profilin–actin and instead mainly recruits uncomplexed G-actin, which is predominantly the labeled species at the five-fold molar excess of profilin used in this assay. Consistently, after detachment from the WHAMY clusters, these filaments grew with the same speed and brightness as the control filaments. To gain more insight into a possible oligomerization of WHAMY, we performed analytical size exclusion chromatography with purified WHAMY-FL, and obtained a calculated molecular mass of 413 kDa, strongly suggesting oligomerization of the 64-kDa protein, although a precise oligomerization state cannot be calculated from these experiments without knowledge about the shape of the molecule (Fig. S3A,B). Combined, these data reveal only moderate nucleation, but exceptionally fast filament elongation activity of clustered WHAMY, which could be utilized to generate mother filaments for the Arp2/3 complex. In this case, they also support the concept of an inhibitory role of profilin in Arp2/3-complex-mediated actin assembly (Suarez et al., 2015).

WHAMY function promotes macrophage cell spreading and cell protrusions

Next, we analyzed the *in vivo* function of *whamy*. The *whamy* gene is located on the third chromosome at the cytological location 85E8 (Fig. 4A). It consists of four exons encoding three predicted protein isoforms that differ only in their N-termini (FlyBase). The largest protein isoform, $WHAMY^{PC}$ (66 kDa) contains both N-terminal CRIB domains, whereas the shortest isoform $WHAMY^{PB}$ (54.1 kDa) lacks the first CRIB domain (FlyBase). To elucidate the *in vivo* role of WHAMY, we generated mutant flies by imprecise excision mutagenesis utilizing two different P-elements inserted in the 3′-UTR of the *whamy* gene (Fig. 4A).

Journal of Cell Science

Journal of Cell Science (2016) 129, 604-620 doi:10.1242/jcs.179325

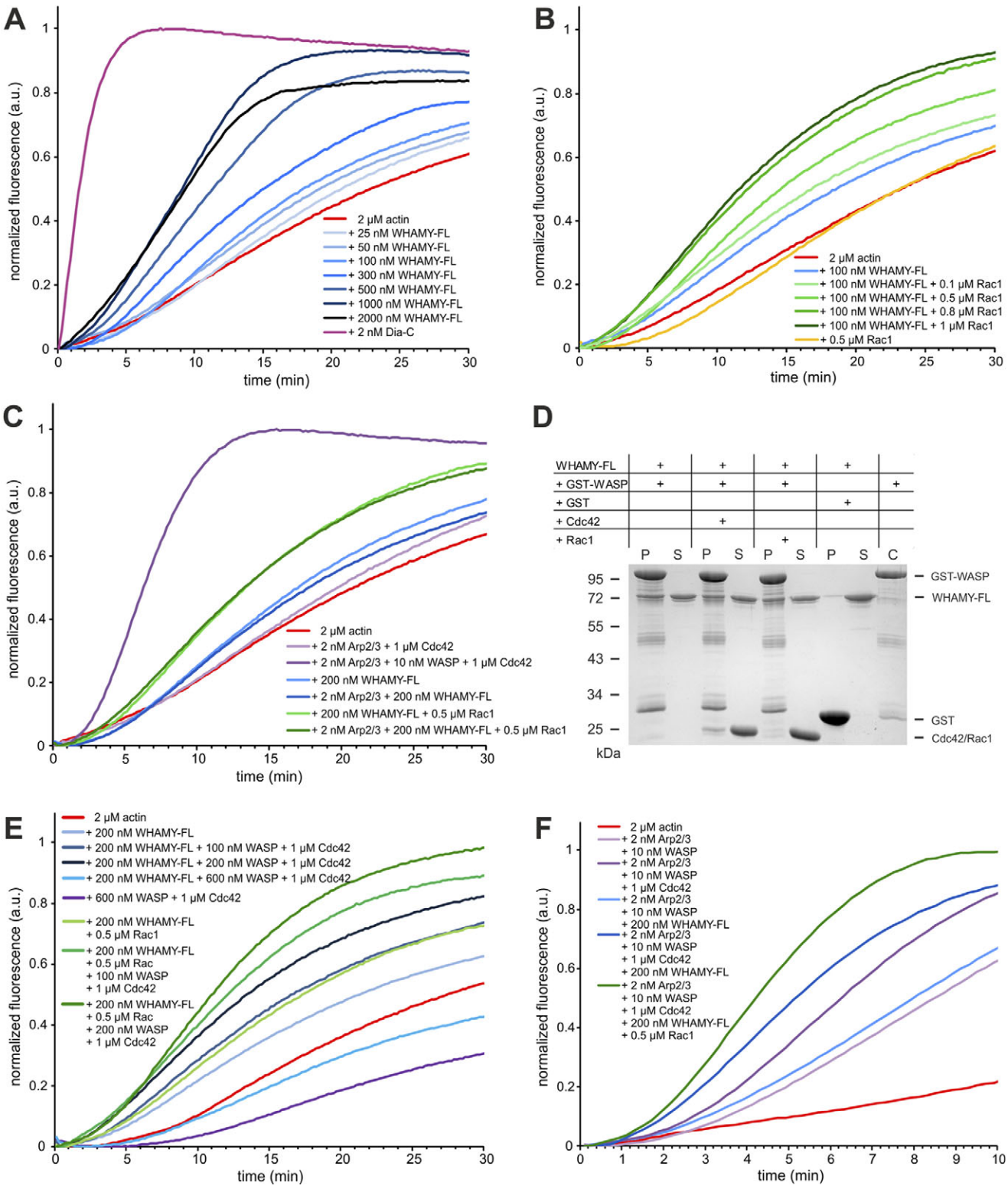

Fig. 2. WHAMY is a new actin assembly factor. (A) WHAMY-FL promotes actin polymerization (2 µM, 5% pyrene labeled) in a concentration-dependent manner. The C-terminal half of Diaphanous (Dia-C) serves as a control for an efficient actin filament nucleation factor. (B) Addition of constitutive active Rac1 further stimulates WHAMY-mediated actin polymerization, whereas the GTPase alone has no effect on actin assembly. (C) WHAMY-FL does not activate the Arp2/3 complex, even when stimulated by active Rac1. In contrast, a low nanomolar concentration of Cdc42-activated WASP is sufficient for prominent activation of the Arp2/3 complex. (D) WHAMY-FL interacts with WASP in pulldown assays. Binding of WHAMY-FL is not increased upon addition of active Cdc42 or Rac1. The Coomassie-Blue-stained SDS-polyacrylamide gel is shown. P, pellet; S, supernatant; C, control. (E) WASP enhances WHAMY-mediated actin polymerization at up to equimolar concentrations. This effect is more pronounced in the presence of active Rac1. Higher concentrations of WASP lead to decreased actin polymerization rates presumably due to monomer sequestration. (F) Arp2/3-complex-driven actin polymerization mediated by Cdc42-activated WASP is further enhanced by addition of WHAMY-FL and active Rac1, but WHAMY alone is not sufficient to fully activate the NPF-activity of WASP. Results are representative of *n*=4, except for D in which *n*=3.

Journal of Cell Science

Journal of Cell Science (2016) 129, 604-620 doi:10.1242/jcs.179325

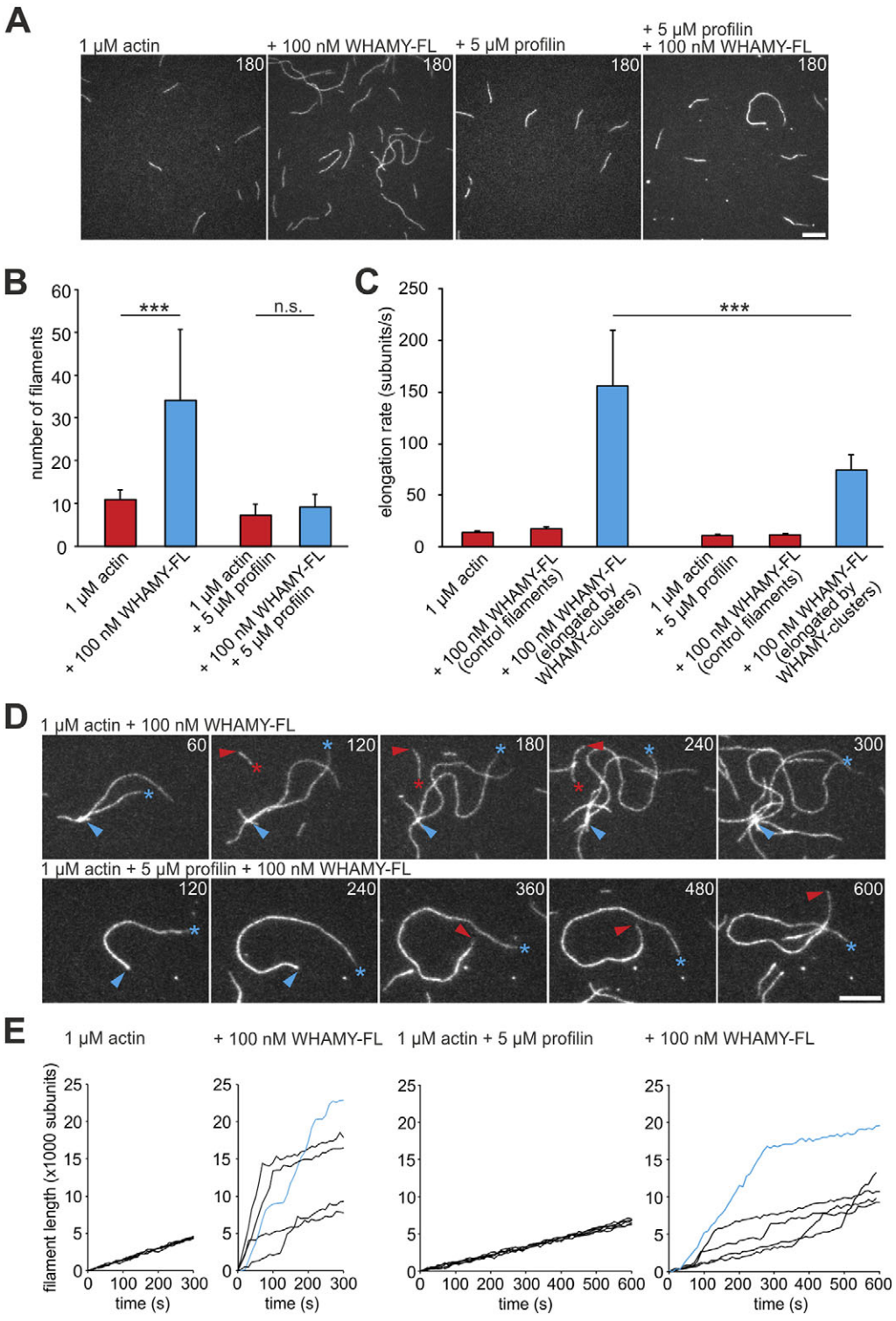

Fig. 3. WHAMY promotes rapid actin filament elongation. (A) WHAMY-FL nucleates filaments in the absence of profilin–actin. Representative single-filament TIRF micrographs are shown. Time is in seconds. Scale bar: 10 µm. (B) Quantification of filaments recorded by single-filament TIRF microscopy. Bars represent mean±s.d. ***P<0.001; n.s., not significant (t-test). The nucleation efficacies were obtained by counting and averaging the number of nucleated actin filaments in an area of 80 µm×80 µm after 3 min at two positions in three independent experiments. (C) WHAMY-FL rapidly elongates barbed ends of actin filaments. Elongation rates of barbed ends associated with WHAMY-FL (blue) compared to elongation rates of control filaments (red) in presence and absence of profilin. Bars represent mean±s.d. ***P<0.001 (t-test). The elongation rates of 25 filaments for each experimental condition were measured by manual tracking of growing barbed ends using ImageJ software. (D) TIRF micrographs of WHAMY-FL-elongated actin filaments evaluated in C. Blue arrowheads mark barbed ends associated with WHAMY clusters; red arrowheads mark free barbed ends growing at the control rate. Asterisks mark respective pointed ends. Note that barbed ends elongated by WHAMY-FL in presence of profilin appear brighter than control filaments. After dissociation of WHAMY-FL, these barbed ends continue to grow with the rate and brightness of control filaments (see also Movie 4). Time is in seconds. Scale bar: 10 µm. (E) Length over time plots of filaments recorded by TIRF microscopy. WHAMY-FL elongated filaments shown in D are marked in blue.

We isolated two deletions, *whamy*$^{\Delta 109}$ and *whamy*$^{\Delta 65}$, removing either the third and fourth exon as well as parts of the second exon. Reverse transcriptase (RT)-PCR and western blot analyses confirmed a loss of WHAMY expression in *whamy*Δ109 and *whamy*Δ65 deletion mutants (Fig. 4B; Fig. S3C). In wild-type extracts, a distinct WHAMY-specific protein band was detected at ~60 kDa (Fig. 4B).

Remarkably, flies with all *whamy* alleles in homozygosity and trans-heterozygosity were viable and fertile with no obvious morphological defects. Hence, we conclude that WHAMY is not essential for *Drosophila* development, but rather might regulate cell-type-specific actin-dependent processes. High-throughput expression data indicate that WHAMY is most abundant in the larval and adult gut, and more weakly expressed in Malpighian tubules and fat body (FlyAtlas, anatomical expression database), but low expression is also found in hemocyte-like S2 cells and tumorous blood cells mbn2 (modENCODE cell line expression database). Therefore, we further analyzed the cellular WHAMY function in

Journal of Cell Science

Journal of Cell Science (2016) 129, 604-620 doi:10.1242/jcs.179325

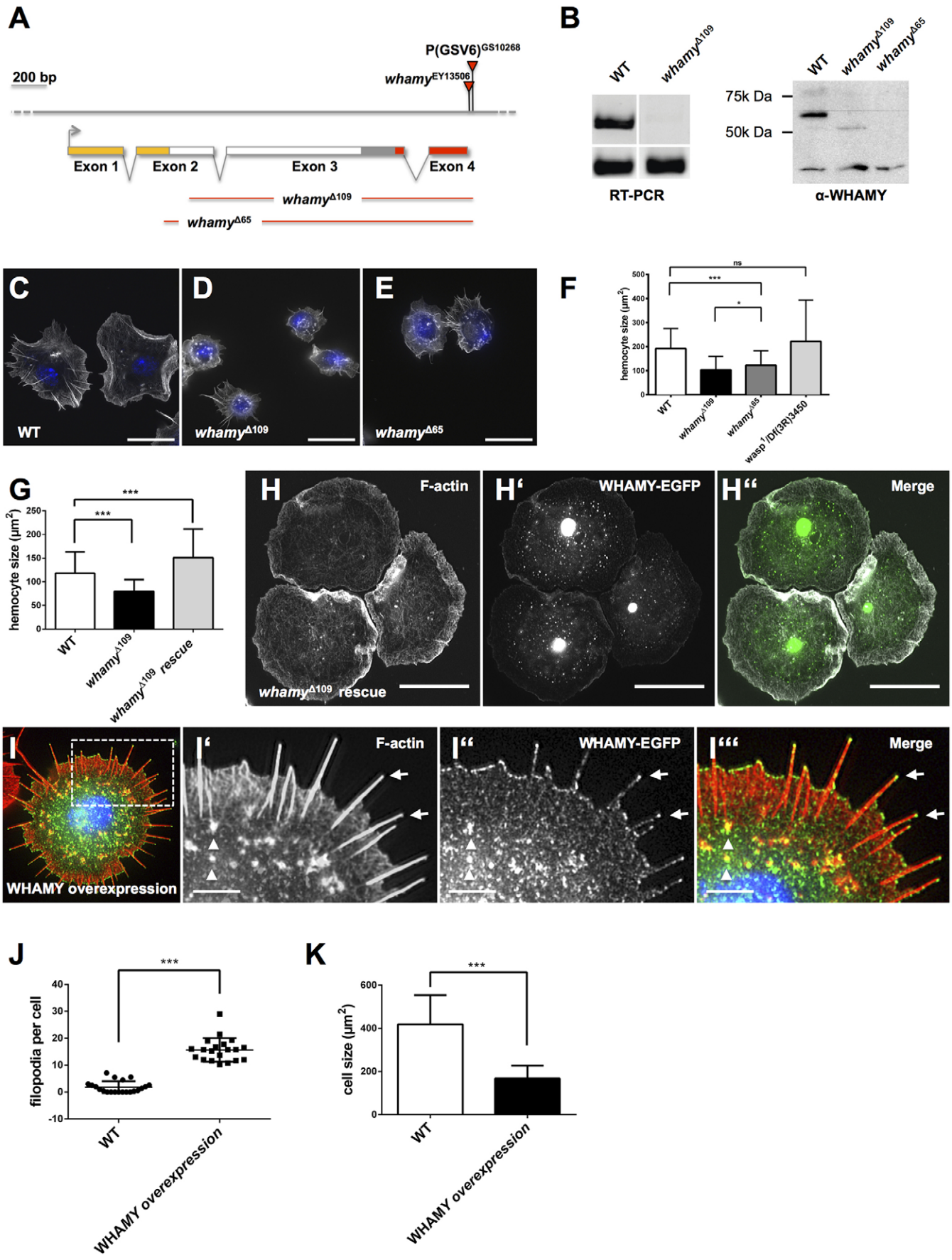

Fig. 4. See next page for legend.

Journal of Cell Science

Journal of Cell Science (2016) 129, 604-620 doi:10.1242/jcs.179325

Fig. 4. WHAMY function promotes cell spreading and cell protrusions. (A) Schematic overview of the *whamy* gene locus. The *whamy* gene is localized on the third chromosome in the cytological region 85E8-E8. The P-element insertions P{EPgy2}Whamy^{EY13506} and P{GSV6}GS10268 are indicated by the red triangles. The breakpoints of the *whamy* deletions (Δ109, Δ65) induced by P-element excision are indicated. The exons of the largest *whamy* isoform (PB) are colored according to the encoding domains (orange, CRIB domains; gray, proline-rich; red, WH2 domains). (B) RT-PCR (left) and western blot (right) analyses of cell lysates obtained from wild-type (WT) and homozygous *whamyΔ*109, *whamyΔ*65 mutant adult guts confirm the complete loss of WHAMY expression. Loss of expression in *whamy* mutants was confirmed in three independent western blot experiments. (C–E) Representative SIM images of isolated (C) wild-type and (D,E) *whamy* mutant pupal macrophages stained with phalloidin (white, F-actin) and DAPI (blue, nuclei). Scale bars: 10 µm. (F) Quantification of the cell spread area of wild-type and mutant macrophages plated on uncoated cover slips. *n*=300 WT, *n*=298 *whamy*^{Δ109}, *n*=175 *whamy*^{Δ65}, *n*=208 wasp^{1}/Df(3R)3450. Bars represent mean±s.d. **P*<0.01, ****P*<0.0001 (Kruskal–Wallis and Dunn's multiple comparison test; ns, not significant). (G) Quantification of cell spread area of wild-type, *whamy*^{Δ109} mutant and rescued macrophages plated on uncoated cover slips. The flies for this experiment were kept at 29°C to enhance the weak WHAMY–EGFP expression. *n*=210 WT, *n*=204 *whamy*^{109}, *n*=301 *whamy*^{Δ109} rescue. Bars represent the median±interquartile range. ****P*<0.0001 (Kruskal–Wallis and Dunn's multiple comparison test). (H–H″) Representative SIM images of rescued *whamy* ^{Δ109} macrophages re-expressing WHAMY–EGFP (green) stained with phalloidin (white, F-actin). Scale bars: 10 µm. (I–I‴) SIM images of isolated wild-type macrophages overexpressing WHAMY–EGFP (green) stained with phalloidin (red, F-actin) and DAPI (blue, nuclei). Arrows mark WHAMY–EGFP on the tips of induced filopodia. Arrowheads mark WHAMY–EGFP and F-actin on vesicles. Scale bars: 3 µm. (J) Quantification of the number of filopodia induced by WHAMY overexpression. Cells were plated on concanavlin A (ConA)-coated coverslips. Bars represent mean±s.d. *P*-values were calculated using the Mann–Whitney test. ****P*<0.0001 (Mann–Whitney test). For quantification, *n*=92 WT and *n*=91 WHAMY–EGFP-expressing cells were measured. (K) Quantification of the reduced cell size upon WHAMY overexpression. Cells were plated on ConA-coated cover slips. Bars represent mean±s.d. ****P*<0.0001 (*t*-test). *n*=83 WT, *n*=89 WHAMY–EGFP.

larval and pupal blood cells, an excellent model system for studying functions of genes involved in actin dynamics at a single-cell level (Sander et al., 2013).

Isolated macrophage-like blood cells showed a broad lamellipodial actin filament network when spread on cover glasses (Fig. 4C). In contrast, *whamy*-deficient macrophages displayed strong defects in cell flattening and cell spreading resulting in significantly smaller cells (Fig. 4D,E, quantification in Fig. 4F). Re-expression of a WHAMY–EGFP transgene in homozygous *whamy*^{Δ109} mutant macrophages rescued the cell-spreading defects, indicating that the defects resulted from a loss of WHAMY function (Fig. 4G). Similar to transfected S2R+ cells, WHAMY–EGFP localized at the leading edge and at actin-rich vesicles in isolated macrophages (Fig. 4H′,H″). Remarkably, rescued cells even showed an increased cell spreading behavior, indicating that WHAMY promotes cell spreading (Fig. 4G,H). Increasing the levels of WHAMY protein by transgene overexpression in a wild-type background did not further increase cell size; rather, overexpression of WHAMY in fact resulted in a marked reduction of cell size and instead dramatically induces the formation of numerous filopodial protrusions (Fig. 4I, quantification in Fig. 4J,K; Movie 5). Overexpressed WHAMY–EGFP still localized to the lamellipodium and vesicles, and strongly marked the tips of induced filopodia (Fig. 4I–I‴; Movie 5). Elevated levels of WHAMY in a wild-type background also induced a dramatic increase of filopodial protrusions *in vivo* (Movie 6). Thus, we propose that WHAMY-mediated actin assembly is required for cell spreading and membrane protrusions of *Drosophila* blood cells. Given that *wasp* mutant cells showed no defects in cell spreading or membrane protrusions (Fig. 4F), WHAMY seems to have acquired a new function in cell motility during evolution.

WHAMY function is important for macrophage cell motility *in vivo*

We next dissected the function of WHAMY in migrating macrophages at different pupal stages *in vivo*. Wild-type prepupal macrophages acquired a spread morphology with broad, polarized lamellipodia (Fig. 5A; Movie 7). First, we examined the localization of the WHAMY–EGFP transgene in homozygous *whamy*^{Δ109} mutant cells lacking the endogenous protein. The WHAMY–EGFP transgene efficiently rescued not only the cell spreading defects of isolated mutant cells, but also did not induce the formation of ectopic filopodial protrusions (Fig. 5B; Movies 8 and 9). WHAMY strongly localizes at the leading edge of migrating polarized macrophages (arrows in Fig. 5B, Movies 8 and 9) and in addition marks dynamic vesicular structures in the cell body of migrating cells (arrowheads in Fig. 5B, Movies 8 and 9).

Given the distinct localization of WHAMY at the leading edge of the cell, we further examined a possible role in cell migration. As recently reported, wild-type macrophages started to initiate random single-cell migration 2 h after puparium formation (Moreira et al., 2013) (Fig. 5C; Movie 10). Compared to wild-type cells, *whamy*^{Δ109} mutant cells showed an impaired spread morphology and had a reduced cell size (Fig. 5D, quantification in Fig. 5E; Movie 11). Striking differences were also seen in the migratory behavior of mutant cells. Whereas wild-type cells spread out and dispersed at 2 h after puparium formation (APF), *whamy*^{Δ109} mutant macrophages still remained closely clustered together and formed densely packed groups of single cells (Fig. 5D, quantification in Fig. 5F; Movie 11). Tracking of individual migrating cells revealed a significant reduction in cell speed (Fig. 5G). Control cells migrated with an average maximum speed of 3.3±0.9 µm/min (mean±s.d.), whereas *whamy*^{Δ109} mutant cells migrated considerably slower with an average maximum speed of 1.9±0.7 µm/min (Fig. 5G). This result indicates that WHAMY is required for proper cell spreading and cell migration *in vivo*.

To further elucidate the importance of WHAMY in directed cell migration, we next performed *in vivo* wounding experiments. Macrophages migrate towards a laser-induced wound or after ablation of a single cell (the ablation side is marked by a yellow circle in Fig. 5H,H′; Movie 12). Similar to control cells, *whamy*-deficient cells still polarized in response to wounds and exhibited a directional cell migratory behavior, albeit with significantly reduced speed (Fig. 5I,I′; Movie 13). To quantify changes in directional cell migration, we analyzed the migratory behavior of macrophages in later pupal stages (17 h APF; Fig. 5I,J) by measuring the Histogram-based Macrophage Migration Score (HMMS) that we recently established (Lammel et al., 2014). Macrophages from later pupal stages are more dispersed, migrating in 3D rather than in 2D, as in prepupae, and their wound response is much stronger (Sander et al., 2013; Lammel et al., 2014). HMMS measurements of wild-type and mutant cells confirmed that cells deficient for *whamy* were still able to respond and migrate to wound sites but that their speed was reduced (Fig. 5H–J; Movies 14 and 15). The differences between wild-type and mutant macrophages were most obvious in the first 600 s after wounding, when a rapid response of the wild-type cells compared to *whamy* mutant cells could be measured (Fig. 5J). These data indicate that WHAMY is required for proper cell spreading and cell migration *in vivo*.

Journal of Cell Science (2016) 129, 604-620 doi:10.1242/jcs.179325

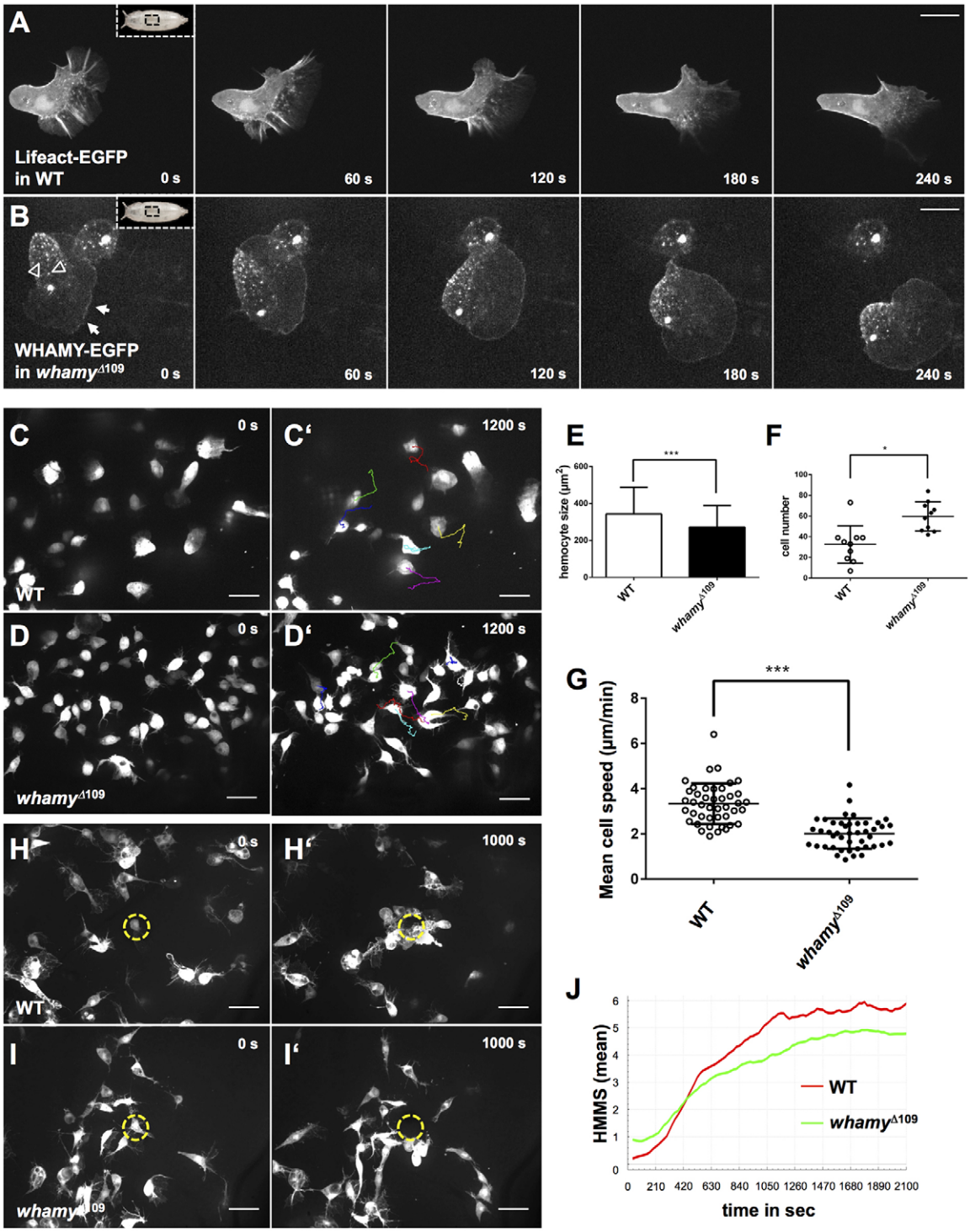

Fig. 5. WHAMY function is important for cell migration. (A) Frames of spinning disk microscopy time-lapse movie (Movie 7) of a migrating wild-type (WT) macrophage expressing transgenic Lifeact–EGFP imaged from a living prepupa (2 h APF). Scale bar: 10 µm. (B) Frames of spinning disk microscopy time-lapse movie (Movie 8) of a migrating *whamy* mutant macrophage re-expressing WHAMY–EGFP imaged from a living prepupa (2 h APF). Scale bar: 10 µm. (C,D) Frames of spinning disk microscopy time-lapse movie of migrating wild-type (C,C′) and *whamy* mutant (D,D′) macrophages at indicated time points, visualized by the expression of cytoplasmic EGFP. Cells were tracked for 20 min (10 s time intervals). Migratory tracks of individual cells are indicated (colored lines). Scale bars: 20 µm. (E) Quantification of the reduced cell size in *whamy*$^{\Delta 109}$ mutant macrophages *in vivo*. n=107 (WT), n=179 (*whamy*$^{\Delta 109}$). Bars represent mean±s.d. ***P<0.0001 (Mann–Whitney test). (F) Quantification of increased macrophage number in living *whamy*$^{\Delta 109}$ prepupae (2 h APF) *in vivo*. n=10 pupae. Bars represent mean±s.d. *P<0.01 (t-test). (G) Quantification of the mean cell speed of randomly migrating wild-type and *whamy* mutant macrophages 2 h after puparium formation. n=43 cells (WT), n=44 cells (*whamy*$^{\Delta 109}$). Bars represent mean±s.d. ***P<0.0001 (Mann–Whitney test). (H,H′,I,I′) Migrating wild-type (H,H′) and *whamy* mutant (I,I′) macrophages (19 h APF) show a migratory behavior towards the wound (indicated by the yellow circle) (see also Movies 12–15). Scale bars: 20 µm. (J) Mean HMMS values for wild-type (red, n=5) and *whamy* mutant (green, n=9) macrophages (20 h APF) plotted for 2100 s after wounding. An overall higher mean HMMS value is observed for the wild-type cells compared to *whamy* mutant cells, indicating more and faster movement towards the wound over time. See also Movies 14 and 15.

Journal of Cell Science

Journal of Cell Science (2016) 129, 604-620 doi:10.1242/jcs.179325

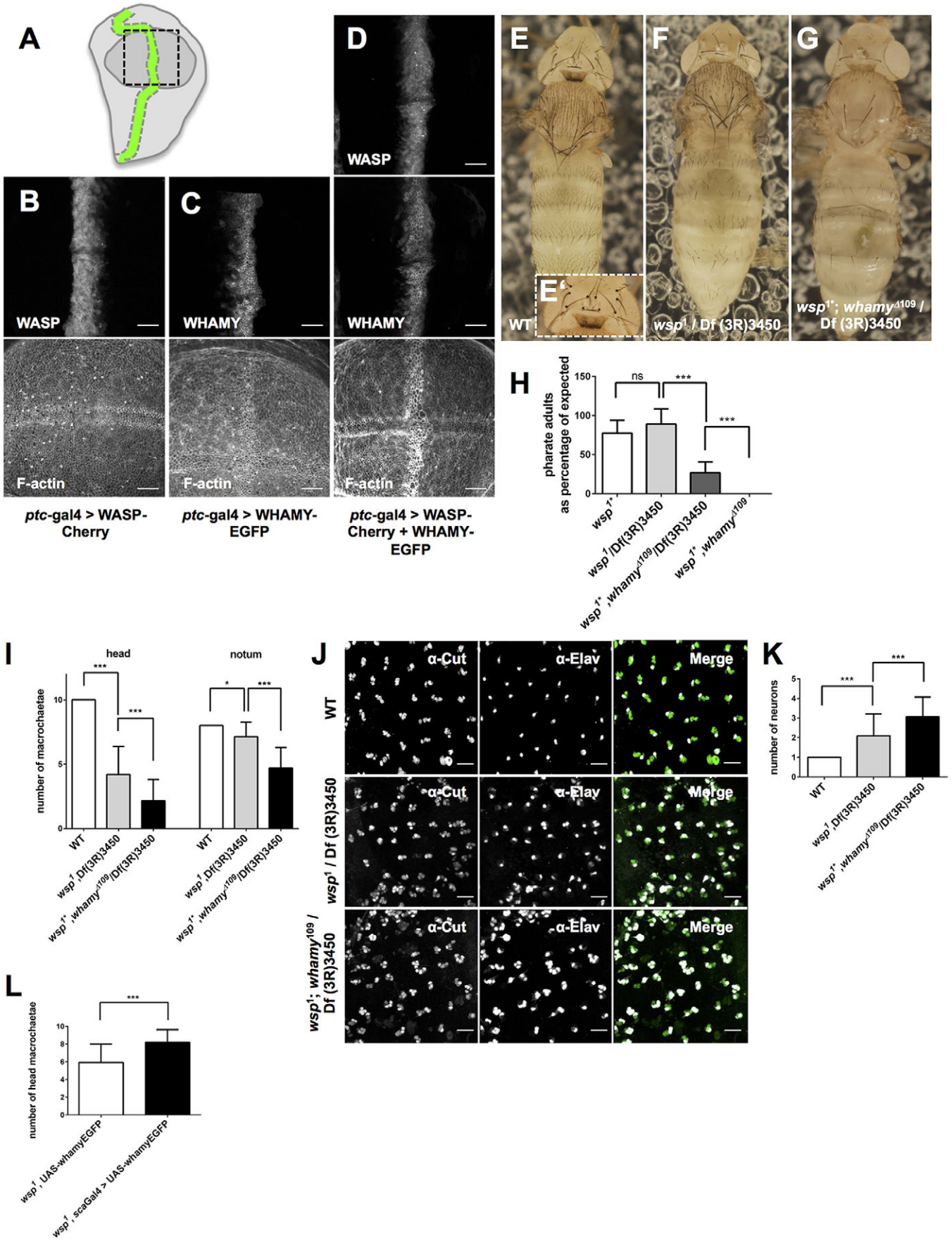

Fig. 6. See next page for legend.

Journal of Cell Science

Journal of Cell Science (2016) 129, 604-620 doi:10.1242/jcs.179325

Fig. 6. WHAMY and WASP cooperatively function in cell fate specification. (A) Schematic drawing of the *ptc-gal4* domain of third-instar wing imaginal discs, which drives expression in a stripe at the anterior–posterior boundary. (B) Expression of WASP has no effects on F-actin. (C) WHAMY alone has only mild effects on F-actin, whereas (D) co-expression of WHAMY and WASP in the *ptc-gal4* domain stimulates F-actin formation. Scale bars: 20 µm. (E–G) Pharate adults of the indicated genotypes. Loss of zygotic *wasp* function results in an apparent reduction of microchaetae and macrochaetae on the head capsule and abdomen. The numbers of macrochaetae on the thorax are only slightly affected. Heterozygous loss of *whamy* strongly enhances the *wasp* mutant bristle-loss phenotype, the overall number of microchaetae and macrochaetae are dramatically reduced. (E′) Wild-type head macrochaetae quantified in I and L. (H) The percentage of pharate adults with respect to the expected number of offspring was calculated. *n*=14 crosses, wsp^{1*}; *n*=15 crosses, wsp^{1}/Df(3R)3450; *n*=20 crosses, $whamy^{\Delta 109}$,wsp^{1*}/Df3450 and *n*=18 crosses, wsp^{1*}, $whamy^{\Delta 109}$ homozygous. Bars represent mean±s.d. ***P<0.0001; ns, not significant (ANOVA). (I) Quantification of the bristle-loss phenotype on the head capsule and notum of newly eclosed *wsp* and heterozygous *whamy*, *wasp* double mutant flies. *n*=30; Bars represent mean±s.d. *P<0.01; ***P<0.0001 (one-way ANOVA for the head macrochaetae and Kruskal–Wallis and Dunn's multiple comparison test for the thorax macrochaetae). (J) Confocal micrographs of pupal notae reveal that the enhanced loss of external sensory bristle structures is due to an excess of neurons. The wild-type four-cell formations (visualized with anti-Cut antibody) are clearly affected in homozygous wasp mutants, but this phenotype is strongly enhanced in heterozygous *whamy*, *wasp* double mutants. Double labeling with Cut (green) and Elav (red), which stain neuronal nuclei, demonstrates that nearly all sensory organ cells in the heterozygous *whamy*, *wasp* double mutants express the neuronal markers. (K) Quantification of the neurogenic phenotype by counting Elav-positive neurons. *n*=100 SOC (sensory organ cells); Bars represent mean±s.d. ***P<0.0001 (Kruskal–Wallis and Dunn's multiple comparison test). (L) The bristle-loss phenotype in *wasp* mutants can partially be rescued by expression of WHAMY–EGFP in all proneural clusters (by means of sca-Gal4). Macrochaetae on the head capsule were counted. *n*=46 animals, wsp^{1}, UAS-whamyEGFP; *n*=42 animals, wsp^{1}, *sca*Gal4>UAS-whamyEGFP; Bars represent mean±s.d. ***P<0.0001 (Student's *t*-test).

WHAMY and WASP act cooperatively in sensory organ development

Given the observed *in vitro* WHAMY–WASP interaction, we next conducted co-overexpression experiments *in vivo* using the Gal4-UAS system (Brand and Perrimon, 1993). Forced expression of full-length WASP in wing imaginal disc epithelium did not induce actin assembly, suggesting that WASP is strongly auto-inhibited *in vivo* (Fig. 6B). WHAMY overexpression only slightly increased F-actin formation (Fig. 6C). However, co-overexpression of WHAMY and WASP strongly induced F-actin (Fig. 6D), suggesting that there are synergistic functions of both proteins *in vivo*. How might WHAMY and WASP act together *in vivo*? In S2R+ cells, we found not only an interaction between a WHAMY–EGFP and a WASP–Cherry fusion but also a striking colocalization at vesicles (Fig. S4A,B). However, there was no overlap at the leading edge of S2R+ cells, suggesting a common function of WHAMY and WASP in vesicle trafficking (Fig. S4A).

To further test functional interactions *in vivo,* we analyzed trans-heterozygous and homozygous double mutants. For this analysis we used the wsp^{1} allele, which contains a small intragenic deletion resulting in a premature stop codon (Ben-Yaacov et al., 2001). As for all other EMS-induced *wasp* alleles, the chromosome carrying the $wasp^{1}$ allele also contains additional lethality-causing mutations. Therefore, we used transheterozygous combinations with the deficiency Df(3*R*)3450, which completely removes, among others, the *wasp* gene (Ben-Yaacov et al., 2001). wsp^{1}/Df(3*R*)3450 transheterozgygotes survived until early adulthood, but many mutant flies failed to fully eclose from the pupal case. Escaper flies exhibited a lack of sensory microchaetes and macrochaetes (Ben-Yaacov et al., 2001). To analyze *wasp*, *whamy* double mutant flies, we cleaned the wsp^{1} allele from associated lethal mutations (designated as wsp^{1*}) and generated recombinant flies carrying the wsp^{1} and the $whamy^{\Delta 109}$ allele (wsp^{1*}, $whamy^{\Delta 109}$). Homozygous wsp^{1*} flies survived as wsp^{1}/Df(3R)3450 transheterozgygotes until early adulthood with no significant phenotypic differences (Fig. 6H). However, homozygous wsp^{1*}, *whamy* double mutants were late-embryonic lethal with very few larval escapers (Fig. 6H). Even the loss of one *whamy* gene copy in wsp^{1*}/Df(3R)3450 transheterozgygotes (wsp^{1*}, $whamy^{\Delta 109}$/Df(3R)3450) significantly shifted the lethality from late pupal or adult to early larval stages (Fig. 6H). These animals survived until late pupal stage (pharate adults) but all failed to eclose from the pupal case and show an enhanced loss of sensory bristles phenotype compared to homozygous or hemizygous wsp^{1*} mutants (compare Fig. 6E–G, quantification of the increased lethality in Fig. 6H). Quantification of this neurogenic phenotype revealed that the formation of the sensory bristles was strongly affected, similarly to what is observed for *arp2/3* mosaics (Fig. 6I; Rajan et al., 2009).

Double staining of pupal nota dissected at 24 h APF with the neuronal nuclear marker Elav, and Cut, which mark all sensory organ precursor cells, confirmed that the enhanced loss of external sensory bristle structures was due to an increased excess of neurons (Fig. 6J). In wild-type flies, each sensory organ precursor cell (SOP, pI cell) normally undergoes an asymmetric cell division to generate two different daughter cells (pIIa and pIIb). The pIIa cell divides to generate the external sensory organ cells, the shaft and socket cells, whereas the pIIb cell undergoes two additional asymmetric cell divisions to generate the internal sensory organ cells including the neuron, the sheath cell and a glial cell (Gho et al., 1999). WASP–Arp2/3-mediated actin nucleation seems to be required for both cell fate decisions. *wasp* mutants frequently showed a pIIa-to-pIIb cell fate transformation resulting in a duplication of neurons (Ben-Yaacov et al., 2001; Fig. 6J). By contrast, trans-heterozygous *wasp*, *whamy* double mutants had, on average, three Elav-positive neurons per sensory organ (Fig. 6J,K). Thus, WHAMY and WASP function cooperatively during sensory organ development. Given the observed synergistic effects of WHAMY and WASP on actin assembly, we further tested whether WHAMY expression could complement *wasp* function. We found that forced expression of WHAMY in *wasp* mutant sensory clusters using the *scabrous* Gal4 driver resulted in a weak but significant increase of sensory bristles (Fig. 6L). Therefore, WHAMY can partially substitute for WASP functions in sensory organ development.

whamy and *wasp* are required for myoblast fusion during embryonic muscle formation

The strong synergistic defects of trans-heterozygous mutants raise the issue of whether the late-embryonic lethality of *whamy*, *wasp* double mutants is caused by cell fate decision defects during sensory organ development as previously shown for embryos lacking both maternal and zygotic WASP (Ben-Yaacov et al., 2001). However, we found no significant changes in the number of neurons in the mature embryonic PNS of *whamy*, *wasp* double mutants. Given that WASP function is further required for multinucleated muscle formation during embryogenesis and for the attachment of muscles to epidermal tendon cells (Massarwa et al., 2007; Schafer et al., 2007), we further analyzed possible defects during muscle development. Remarkably, single *whamy* and *wasp* mutants showed similar attachment defects of the longitudinal transverse muscles (Fig. 7B,C, arrows). By contrast, *whamy*, *wasp* double

Journal of Cell Science

Journal of Cell Science (2016) 129, 604-620 doi:10.1242/jcs.179325

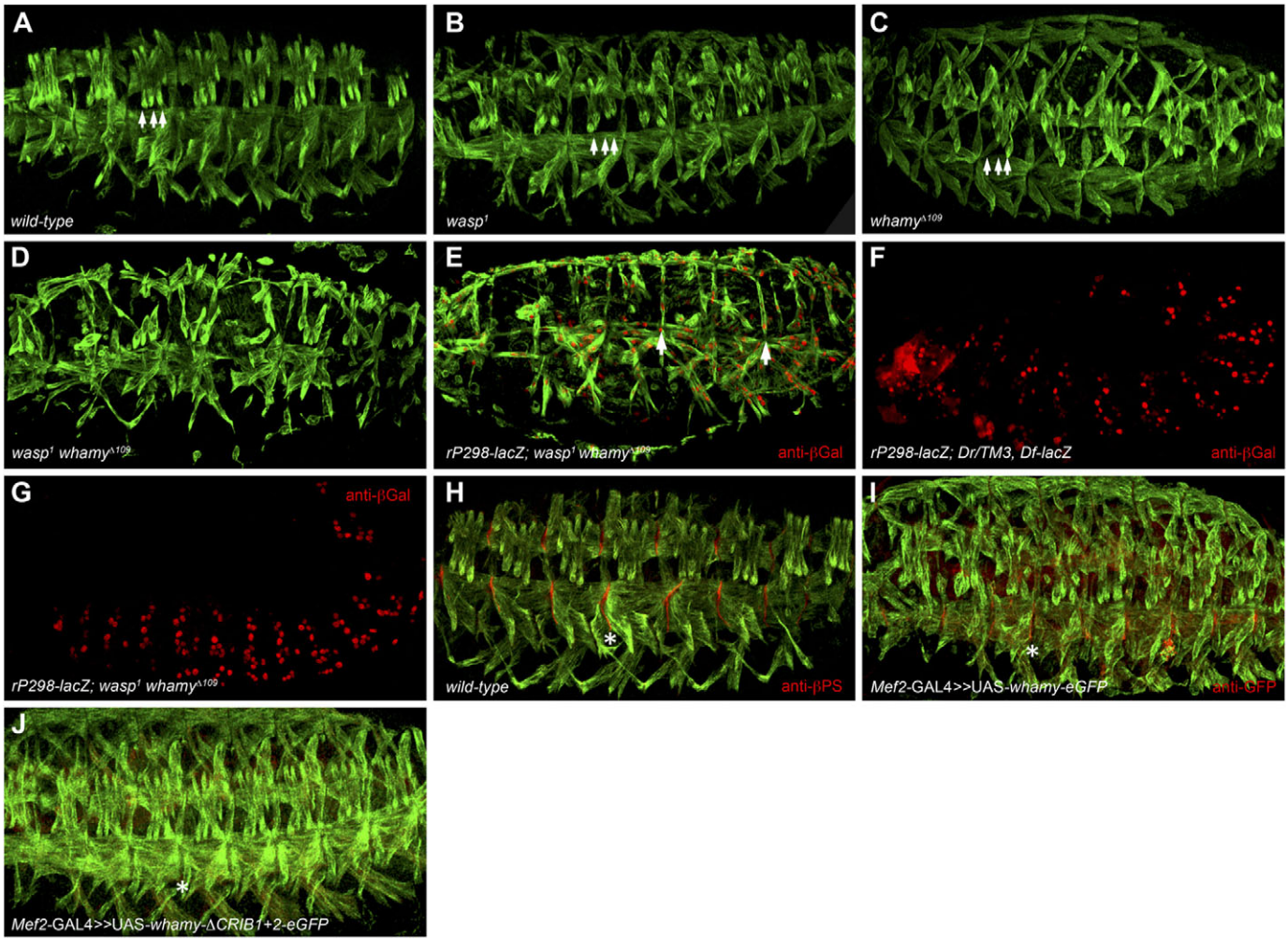

Fig. 7. WHAMY and WASP cooperatively function in myoblast fusion. (A–E,H–K) Lateral view of stage 16 embryos immunostained with anti-β3-Tubulin antibody. (A) Longitudinal transverse muscles are correctly attached in wild-type musculature (arrows). (B,C) Homozygous *wsp*^{1} and *whamy*$^{\Delta 109}$ single mutant embryos display attachment defects of lateral muscles (arrows). (D,E) Homozygous *wasp*^{1}, *whamy*$^{\Delta 109}$ double mutants with disturbed muscle pattern. (E) *rP298*-lacZ expression in the background of a homozygous *wsp*^{1}, *whamy*$^{\Delta 109}$ mutant embryo. Arrows point towards the segmental border muscle. (F) Stage 11 embryos carrying the enhancer trap line rP298 and the blue balancer chromosome TM3 *Deformed*–lacZ. (G) Stage 12 *wsp*^{1}, *whamy*$^{\Delta 109}$ mutant embryo carrying the enhancer trap line rP298. (H) Wild-type embryo stained with anti-β3-Tubulin and anti-Integrin βPS antibodies to mark attachment sites (asterisk). (I) Expression of WHAMY–EGFP under the control of the *Mef2*-GAL4 driver. WHAMY–EGFP is enriched at muscle attachment sites (asterisk). (J) WHAMY localization at muscle attachment sites depends on its CRIB domains. Embryos expressing WHAMY-ΔCRIB1+2 in myoblasts with *Mef2*-GAL4 show no longer an enrichment of WHAMY at muscle attachment sites (asterisk).

mutants displayed strong defects in muscle size and morphology (Fig. 7D). Multinucleated muscle formation depends on the fusion of two myoblast populations: founder cells and fusion-competent myoblasts (FCMs). Founder cells initiate muscle formation by attracting FCMs for the fusion process (Bate, 1993). They further determine the position, size, orientation, epidermal attachment site of the muscle and patterns of innervation (Bate, 1993). The selection of founder cells depends on Notch-mediated lateral inhibition (Carmena et al., 1995). To further characterize the double mutant phenotype in more detailed, we crossed the *rP298*-lacZ enhancer trap line that marks the nuclei of founder cells into the background of *whamy*, *wasp* double mutants (Nose et al., 1998). In stage 16 embryos, we found that the segmental border muscle contained only one to two nuclei (Fig. 7E, arrows), instead of up to seven nuclei, like in wild-type embryos (Bataille et al., 2010). This finding indicates that myoblast fusion is disturbed in *whamy*, *wasp* double mutants. To rule out that this phenotype is based on founder cell specification defects, we compared *rP298*-lacZ expression at stage 11 embryos of wild-type and *whamy*, *wasp* double mutants when myoblasts start to fuse. In both, we observed a comparable number of *rP298*-lacZ-expressing cells, suggesting that the majority of founder cells are specified correctly (Fig. 7F,G). To determine whether WHAMY localizes, like WASP, at the contact site of adhering myoblasts (Schafer et al., 2007; Deng et al., 2015), we expressed the WHAMY–EGFP transgene in all myoblasts by using the *Mef2*-GAL4 driver line. We indeed could detect WHAMY–EGFP at the myoblast membrane, but failed to observe a distinct localization of WHAMY at the contact site of myoblasts. Instead, we noticed the expression of WHAMY–EGFP at the attachment sites (Fig. 7H,I, asterisks). A similar distribution has been reported for WASP (Schafer et al., 2007). Interestingly, the localization of WHAMY to muscle attachment sites was lost when a WHAMY deletion that lacked both CRIB domains was expressed in all myoblasts (Fig. 7J). Thus, both CRIB domains seem to be essential for the localization of WHAMY to attachment sites, but this does not seem to disturb muscle attachment (Fig. 7J). Taken together, these

Journal of Cell Science

Journal of Cell Science (2016) 129, 604-620 doi:10.1242/jcs.179325

data indicate that WASP and WHAMY synergistically function in embryonic myoblast fusion, muscle attachment and adult sensory organ development.

DISCUSSION

WHAMY – evolution of new genome functions by duplication and subneofunctionalization

The identification of all WASP family homologs in all sequenced organisms allows a detailed phylogenetic analysis of the origin of diverse subfamilies evolving differential cellular functions. WASP proteins are multi-domain proteins. They share functions that are encoded by similar domains at the C-termini, whereas different N-terminal domains mainly define their diverse cellular processes. Gene duplication and domain shuffling are two important mechanisms driving novel and increasingly complex developmental programs during evolution (Babushok et al., 2007; Buljan and Bateman, 2009). It is thought that this boost in domain shuffling is responsible for the apparent disconnection between greatly increased phenotypic complexity and a relatively small difference in gene number between humans and *Drosophila* (Babushok et al., 2007; Claverie, 2001).

The *whamy* gene is an excellent example for how gene duplication and subsequent domain shuffling can create new gene functions after initial gene duplication. It arose through a duplication of *wasp* at the base of the genus *Drosophila*. Although the encoded protein has evolved a new function in cell motility, it also functions synergistically with WASP in muscle formation and sensory organ development. In the latter, WHAMY can even partially substitute for WASP, indicating that it has kept functionality following the duplication. This duality is reflected in the sequence of the WHAMY CRIB domains. As there is an overlap in function with WASP, selective pressure has been reduced since the duplication, leading to the observed increase of evolutionary rate. Following the duplication of the CRIB domains within WHAMY, a similar trend can be found. Whereas one domain has kept the function of binding to Cdc42-GTP, the other has lost the ability to interact. This is reflected in domain-specific conserved substitutions. The duplication of the *wasp* gene and subsequent subneofunctionalization of *whamy* might have occurred at the same time as the loss of a true WHAMM/JMY ancestor during insect evolution (Veltman and Insall, 2010). Like *Drosophila* WHAMY, the common ancestor of WHAMM/JMY proteins in invertebrates also lacks the characteristic C-terminal tryptophan residue in their VCA domains that is crucial for Arp2/3 binding and activation (Veltman and Insall, 2010). This further implies a primary Arp2/3-independent function of the common ancestor of invertebrate WHAMM/JMY proteins.

WHAMY – a new actin polymerase regulating cell motility

WHAMY shows no Arp2/3-activating NPF activity *in vitro*. However, different from WASP, WHAMY itself is able to promote fast elongation of linear actin filaments from actin-rich clusters. With respect to its activity, WHAMY resembles the WH2-domain containing Ena/VASP polymerases that actively drive processive actin-filament elongation and promote assembly of both lamellipodial and filopodia actin networks (Breitsprecher et al., 2008, 2011; Hansen and Mullins, 2010). Notably, Ena/VASP proteins are tetramers, and their oligomerization is mandatory to allow for polymerase activity in experiments in solution, as used in this study (Breitsprecher et al., 2008). As we have exclusively observed fast filament elongation from WHAMY clusters in our TIRF experiments, and consistent with the size exclusion chromatography experiments, we propose that WHAMY requires oligomerization to acquire actin polymerase activity. Concerning previously analyzed proteins of the WASP family, the filament elongation activity of WHAMY is therefore rather unique, and when compared to other fast actin polymerases, only the *Drosophila* formin Diaphanous achieves comparable high elongation activity *in vitro* (Yan et al., 2013). As evidenced from the pyrene data, the activity of WHAMY can further be increased by Rac1.

Rac1 seems to act on both the activity and the localization of WHAMY at lamellipodial tips. Both of the two CRIB domains of WHAMY bind equally to activated Rac1, and only loss of both CRIB domains abolishes Rac1 binding and the localization to the leading edge. Therefore, it currently remains unclear why WHAMY contains two CRIB domains and whether they differentially mediate distinct cellular functions. They might contribute to a local clustering of WHAMY and Rac1 at the leading edge. The most prominent Rac1 effector represents the WAVE regulatory complex (WRC) that drives Arp2/3-mediated branched actin nucleation. Rac1 directly binds and activates the WRC by allosterically releasing the bound Arp2/3-activating WCA domain of WAVE (Chen et al., 2010; Eden et al., 2002). Overexpression of WHAMY leads to a strong induction of filopodia, presumably due to the filament elongation activity of WHAMY. Additionally, competition between WHAMY and the WRC for Rac1 could disturb the balance between nucleation and elongation activity, and therefore might contribute to the observed overexpression phenotype. Different from WHAMY, WRC function is essential for lamellipodia formation and cell migration in most eukaryotic cells (Pollitt and Insall, 2009). By contrast, loss of WHAMY function does not impair lamellipodia formation but rather regulates cell spreading and contributes to cell motility.

WHAMY and WASP cooperatively control sensory organ development and myoblast fusion

WHAMY does not compete but rather functions together with WASP in *Drosophila* morphogenesis. Previous studies have revealed that the major established activators of WASP, such as Cdc42 and PIP_2, are not required for the function of WASP in sensory organ development or myoblast fusion (Tal et al., 2002). This observation already suggests that additional components, such as WHAMY, might act together with WASP in sensory organ development and myoblast fusion. Consistent with this, we found that further reduction of *whamy* function in *wasp* mutants phenocopies loss of *arp*2/3 function, resulting in an excess of neurons and a near absence of bristle sheath, shaft and socket cells (Ben-Yaacov et al., 2001; Rajan et al., 2009). Our rescue data further indicate that WHAMY can partially substitute for WASP function. Thus, WHAMY cooperates with WASP rather than acting redundantly in sensory organ development. Based on our TIRF microscopy data, we suggest that WHAMY might potentially generate mother filaments in close vicinity of Arp2/3 complex facilitating Arp2/3-mediated actin assembly.

How might WHAMY and WASP act on actin dynamics during sensory organ development? Recent work suggests that the WASP–Arp2/3 pathway is not involved in Notch receptor endocytosis or its processing in the signal-receiving cell (pIIa) but rather plays an important role in the trafficking of Delta-positive vesicles from the basal area to the apical cortex of the signal-sending pIIb cell (Rajan et al., 2009). This model also implies that recycled Notch ligands such as Delta and Serrate are active at apical junctions with actin-rich structures induced by WASP and the Arp2/3 complex (Rajan et al., 2009), which in turn activate apical Notch receptor in pIIa.

Journal of Cell Science

Journal of Cell Science (2016) 129, 604-620 doi:10.1242/jcs.179325

In vivo, WHAMY localizes at dynamic vesicles during sensory organ precursor formation (Movie 16) and, together with WASP, becomes strongly enriched at apical junctions shortly after SOP division (Movie 17). Thus, we propose a scenario in which WASP and WHAMY might act either on the assembly of actin-rich structures or directly promote apical trafficking of Delta through Rab11-recycling endosomes.

A dynamic reorganization of the actin cytoskeleton into distinct cellular structures is also necessary to ensure successful myogenesis. Filopodial protrusions are crucial for the attachment of FCMs to the founder cell and growing myotube, and for the initiation of the fusion process (Ruiz-Gomez et al., 2000; Sens et al., 2010). The recognition and adhesion of myoblasts depends on members of the immunoglobulin superfamily (IgSF) that are expressed specifically in myoblasts in a ring-like structure. The interaction of these proteins leads to the formation of a cell communication structure, which has been termed fusion-restricted myogenic adhesive structure (FuRMAS) or podosome-like structure (Kesper et al., 2007; Richardson et al., 2007; Sens et al., 2010). The cytodomains of the IgSFs trigger the activation of WAVE in founder cells, and of WAVE and WASP in FCMs (Sens et al., 2010; Kaipa et al., 2013). In FCMs, WAVE- and WASP-mediated Arp2/3 activation results in the formation of a dense F-actin focus that accumulates at the interface of adhering myoblasts (Kesper et al., 2007; Sens et al., 2010). Electron microscopy studies have revealed that WASP is required for the formation of fusion pores at apposing myoblasts during embryonic and indirect flight muscle development (Massarwa et al., 2007; Berger et al., 2008, Dhanyasi et al., 2015). These fusion pores expand until full cytoplasmic continuity is achieved, and WASP has implicated to be required for fusion pore expansion (Massarwa et al., 2007). It has been discussed that WASP is required for the removal of membrane residuals during membrane vesiculation. WHAMY might contribute to this process, but the detailed mechanistic contribution of WHAMY in fusion pore formation needs to be addressed in future studies by ultrastructural analyses.

MATERIALS AND METHODS

Drosophila genetics

The following strains were used: w^{1118}, y^{1} w^{67c23}; P{EPgy2} WhamyEY13506, y^{1} w^{67c23}; P{GSV6}GS10268/TM3, hml^{Δ}-Gal4, hmlΔ-Gal4 EGFP, Lifeact–EGFP, neur-Gal4, ptc-Gal4, sca-Gal4, Df(3R)3450 (Bloomington Stock Center, Bloomington, IN) and wsp^{1} (Ben-yaacov et al., 2001). The *whamy* mutant alleles $whamy^{\Delta 109}$, $whamy^{\Delta 65}$ and $whamy^{\Delta 58}$ were generated by imprecise transposon excision. The UAS-whamy transgenes were generated by ΦC31-integrase-mediated integration into the landing site M{3xP3-RFP.attP'}ZH-86FB$^{-/-}$ as described previously (Stephan et al., 2011). Full-length *wasp*, *whamy* and $whamy^{\Delta CRIB}$ fragments were amplified by PCR and cloned into Gateway Entry Vectors (pENTR D-TOPO, Invitrogen). The inserts were sequenced and subcloned into pUASt-attB-rfA-mCherry, pUASt-attB-rfA-EGFP (Drosophila Genomics Resource Center) by LR *in vitro* recombination (Invitrogen) as previously described (Chen et al., 2014). All *Drosophila* strains were kept on standard medium and crosses were performed at 25°C unless otherwise indicated.

Cell culture, cell transfection and pulldown experiments

Drosophila S2R+ cells were propagated in 1× Schneider's *Drosophila* medium as described previously (Fricke et al., 2009). S2R+ cells were transfected as described previously (Kumar et al., 2009). For GST pulldown experiments, GST–Rac1 or GST–Cdc42 was expressed using *E. coli* Rosetta 2 (DE3) (Novagen). Lysis was performed by sonification in 1× PBS, 2 mM $MgCl_2$, 2 mM DTT, 10% glycerin and protease inhibitor cocktail (Roche). After centrifugation, GST proteins were loaded with GDP or GTPγS, as described previously (Fricke et al., 2009), and immobilized on glutathione resin according to the manufacturer's instructions (GE Healthcare). S2R+ cells transfected with pUAST-whamyEGFP, pUAST-whamyΔ^{CRIB1}EGFP, pUAST-whamyΔ^{CRIB2}EGFP or pUAST-whamy$\Delta^{CRIB1+2}$EGFP and Act5cGal4 were harvested and lysed in 1 ml ice-cold lysis buffer (50 mM Tris-HCl pH 7.4, 150 mM NaCl, 1 mM DTT, 1.5 mM $MgCl_2$, 4 mM EDTA, 1% Triton X-100, 10% glycerin, protease inhibitor cocktail). After centrifugation, 500 µl of the cytoplasmic supernatant was added to 50 µl of loaded (GST–Rac1 or GST–Cdc42) glutathione resin. Following incubation for 1 h at room temperature, unbound proteins were washed away using four washes of 1 ml 1× PBS. 20% of the preparation was used per lane on standard SDS-PAGE and was analyzed by western blot analyses. Co-immunoprecipitations were performed as described previously (Bogdan et al., 2005).

Protein purification, western blot analysis and antibodies

GST-tagged WHAMY-FL, WASP and DiaC, as well as constitutively active Rac1-V12 and Cdc-V12 were expressed in *E. coli* strain ArcticExpress after induction with 0.7 mM IPTG at 12°C at an optical density >1.5. The cells were harvested after 20 h and the GST-tagged proteins were purified by affinity chromatography with glutathione-conjugated agarose (Sigma-Aldrich) using standard procedures. The GST tag was subsequently cleaved by PreScission protease (GE Healthcare) overnight, and the proteins were further purified by size exclusion chromatography on an Äkta Purifier System equipped with a HiLoad 26/60 Superdex S200 column (GE Healthcare) The WHAMY- and WASP-rich fractions were pooled, dialyzed against storage buffer (150 mM KCl, 1 mM DTT, 60% glycerol and 20 mM HEPES pH 7.4) and stored at −20°C. The expression and purification of recombinant *Drosophila* profilin was essentially performed as described previously (Breitsprecher et al., 2008). Arp2/3 complex was purified from bovine brain by affinity chromatography using a GST-tagged WCA domain from human WAVE1 coupled to glutathione-conjugated agarose essentially, as described previously (Loisel et al., 1999), and further purified by size exclusion chromatography on a HiLoad 26/60 Superdex S200 column. Rabbit skeletal muscle actin was extracted from acetone powder and purified according to Spudich and Watt, 1971. Fractions of G-actin were labeled with ATTO 488 maleimide (ATTO-TEC) or N-(1-Pyrene)maleimide (Life Technologies) at Cys^{374} according to the manufacturer's protocols.

For western blot analysis, adult guts of third-instar wandering larvae with the indicated genotype were homogenized in lysis buffer (50 mM Tris-HCl pH 7.4, 150 mM NaCl, 1.5 mM $MgCl_2$, 4 mM EDTA, 10% glycerol, 1% Triton X-100, protease inhibitor cocktail). Equal amounts of protein lysates were separated by SDS-PAGE (10%) and analyzed by western blotting. The affinity purified anti-WHAMY antibody was used 1:500. Anti-WHAMY antibodies were generated against Strep-tagged native WHAMY expressed in a cell-free wheat-germ lysate system (RTS 500, 5Prime). Rabbits were immunized with purified proteins (Davids Biotechnologie, Regensburg, Germany). Affinity purification was done as described previously (Zobel et al., 2015).

Actin polymerization assays

Actin polymerization assays were generally performed as described previously (Junemann et al., 2013). Polymerization of 2 µM rabbit skeletal muscle G-actin (5% pyrene-labeled) in 1× KMEI-polymerization buffer (50 mM KCl, 1 mM MgCl2, 1 mM EGTA, and 10 mM imidazole, pH 7.0) in the presence of various concentrations of WHAMY-FL and other proteins as indicated was monitored by a Synergy 4 fluorescence microplate reader (Biotek).

GST pulldown assays with purified proteins

For each experimental condition, 150 µl of glutathione-conjugated agarose bead slurry were first washed three times with ice cold pulldown buffer containing 20 mM HEPES pH 7.4, 50 mM NaCl, 1 mM DTT, 5 mM $MgCl_2$, 2 mM benzamidine and 5% (v/v) glycerol. GST-tagged proteins were diluted in 1 ml pulldown buffer (final concentrations: 3 µM GST–WASP, 10 µM GST, 10 µM GST-Cdc42 and 10 µM GST-Rac1), then clear spun at maximum speed in a tabletop centrifuge for 15 min to remove precipitates.

The supernatants of these protein solutions were then added to the washed beads and incubated for 1 h on a rotating wheel in the cold to allow binding. Subsequently the beads were spun for 2 min at 8000 ***g***, the supernatants were discarded and the beads were incubated with 1 ml of the non-tagged protein solutions (2 µM WHAMY-FL, 10 µM Cdc42 and 10 µM Rac1 in pulldown buffer) for additional 2 h while slowly rotating. After four washing steps with pulldown buffer, bound proteins were eluted from the beads with SDS sample buffer and analyzed by SDS-PAGE.

Analytic size exclusion chromatography

WHAMY-FL and reference proteins from the gel filtration markers kit (Sigma-Aldrich) were diluted in filtration buffer [20 mM HEPES pH 7.4, 150 mM KCl, 1 mM DTT, 5% (v/v) glycerol] and analyzed by size-exclusion chromatography on a Superdex 200 Increase 10/300 GL gel filtration column using an ÄKTA Purifier system (GE Healthcare). Each run was performed three times. The calibration curve was obtained by plotting the decadic logarithm of the molecular mass [log(MW)] for each calibration protein against the ratio of elution volume (Ve) and void volume (Vo), which was 8.4 ml.

In vitro TIRF microscopy

WHAMY-FL (100 nM final concentration) and profilin (5 µM final concentration) were pre-diluted in 1× TIRF buffer [20 mM imidazole pH 7.4, 50 mM KCl, 1 mM $MgCl_2$, 1 mM EGTA, 20 mM β-mercaptoethanol, 0.5 mM ATP, 15 mM glucose, 2.5 mg/ml methylcellulose (4000 cP), 20 µg/ml catalase, 100 µg/ml glucose oxidase]. The assays were started by adding G-actin (1 µM final concentration, 10% Atto488-labeled) and flushing these mixtures into the pre-coated flow chambers (Junemann et al., 2013). Time-lapse recordings were acquired using a Nikon Eclipse TI-E inverted microscope equipped with a TIRF Apo 60× objective and an Ixon3 897 EMCCD camera (Andor). Frames were captured every 2 s for 10 min with an exposure time of 50 ms. Two sectors per experiments were recorded using a motorized microscope stage. The pixel size corresponds to 0.27 µm. The nucleation efficacies were obtained by counting and averaging the number of nucleated actin filaments in an area of 80 µm×80 µm after 3 min at two positions in three independent experiments. The elongation rates of 25 filaments for each experimental condition were measured by manual tracking of growing barbed ends using ImageJ software. The lengths of five filaments for each experimental condition were measured manually every 10 s for a period of 300 s in absence of profilin and for 600 s in presence of profilin using the segmented line tool of ImageJ.

Immunohistochemistry

Pupal thorax epithelia of staged APF pupae were dissected in ice-cold PBS and fixed for 20 min in 4% paraformaldehyde in PBS. Epithelia were permeabilized in 0.15% Triton X-100 in PBS for 1 h, blocked for 1 h in 3% BSA and stained with primary antibody overnight at 4°C and then for 2 h at room temperature with the secondary antibody. Larval wing discs were dissected and stained in the same fashion. The following primary antibodies were used: mouse anti-Cut (1:10, DSHB), rat anti-Elav (1:10, DSHB), anti-Integrin βPS (1:50, DSHB), mouse anti-GFP (1:1000, Invitrogen), rabbit anti-mCherry (1:1000, Invitrogen). Secondary antibodies were Alexa-Fluor-488-, 568- or 647-conjugated anti-rabbit, anti-rat and anti-mouse IgG (1:1000, Invitrogen). F-actin was stained with Alexa-Fluor-647–phalloidin (1:100, Invitrogen). Samples were mounted in Vectashield (Vectorlabs) or Fluoromount (Southern Biotech). The rP298 enhancer trap line (Nose et al., 1998) was used to label muscle founder cells. The polyclonal anti-β3-Tubulin antibody (from rabbit, 1:12,000, Buttgereit et al., 1996) was used to analyze the somatic body wall musculature and a polyclonal anti-β-galactosidase (1:5000) antibody (Cappel) was used to identify balancer-carrying embryos and to visualize rP298–lacZ expression as described previously (Schafer et al., 2007).

Structured illumination microscopy imaging

SIM images were taken with an ELYRA S.1 Microscope (CellObserver SD, 63×/1.4 NA oil-immersion objective; Zeiss) with the software Zen 2010 D (Zeiss). Image acquisition was performed as described previously (Zobel and Bogdan, 2013). For isolation of macrophages, five white pupae or ten third-instar larvae were bled into 400 µl Shields and Sang M3 medium containing 10% FBS and 1× penicillin–streptomycin. The cell suspension was transferred onto a chambered cover glass and cells were incubated for 1 h at 25°C. Cell fixation and phalloidin staining were performed as previously described (Zobel and Bogdan, 2013).

In vivo migration assay of pupae

Live imaging of macrophages in prepupae and in the pupal wing was performed with a CellObserver SD spinning disk microscope (Zeiss) as reported recently (Sander et al., 2013). The cuticles of staged pupae (16 h APF) were completely removed and pupae were placed on the lateral side and glued on glass bottom culture plates. Cells were imaged through a 40× Plan-Apochromat (NA 1.3) oil-immersion objective using an inverted Zeiss Axio Observer.Z1 microscope with a CCD camera (Axiocam MRm camera, 6.45 µm×6.45 µm) and the 488-nm laser line. For wounding assays, we used the UV laser ablation system DL-355/14 direct, from Rapp OptoElectronics. The ZEN software 2012 (Zeiss) was used for acquisition, and Zen as well as Fiji (ImageJ) software was used for processing of the images. For imaging living pupae or isolated macrophages, we used only 25% laser intensity of the 488-nm argon laser to avoid photodamage.

Quantification of *in vivo* macrophage cell migration

Prepupal macrophages were tracked manually using Fiji and the manual tracking plug-in. To quantify the migratory behavior of pupal macrophages we used the Histogram-based Macrophage Migration Score (HMMS) as described recently (Lammel et al., 2014).

Acknowledgements

We thank M. Sander for help during initial cloning of WHAMY constructs and cell transfection experiments. Meike Bechtold and Anna Julia Squarr for critical reading of the manuscript. We also thank the Bloomington Stock Center and VDRC for fly strains. We thank Jörg Grosshans for profilin and Diaphanous expression plasmids.

Competing interests

The authors declare no competing or financial interests.

Author contributions

K.B. generated the *whamy* mutant flies and all constructs, did the initial biochemical work, and performed the molecular and functional analysis of single- and double-mutant flies in sensory organ development and macrophage cell biology. M.W. performed the actin polymerization assay, GST pulldown assays, analytic size exclusion chromatography and the in vitro TIRF analysis. S-F.Ö. analyzed the myoblast fusion and attachment defects of single- and double-mutant flies. J.S. performed the bioinformatic analyses. J.F. oversaw the biochemical work. S.B. oversaw the genetic and cell biological work, and also performed live-imaging experiments on WHAMY-EGFP localization. S.B. supervised and coordinated the work, and wrote the manuscript with assistance from all authors.

Funding

This work was supported by a grant to S.B. from the cluster of excellence 'Cells in Motion' (CIM), and by grants to S.B. from the Heisenberg Program of the Deutsche Forschungsgemeinschaft (DFG). S.B. and J.F. were supported by the SPP1464 priority program of the DFG. S.F.Ö. was supported by the DFG [grant number OE311/4-2].

Supplementary information

Supplementary information available online at
http://jcs.biologists.org/lookup/suppl/doi:10.1242/jcs.179325/-/DC1

References

Abdul-Manan, N., Aghazadeh, B., Liu, G. A., Majumdar, A., Ouerfelli, O., Siminovitch, K. A. and Rosen, M. K. (1999). Structure of Cdc42 in complex with the GTPase-binding domain of the 'Wiskott-Aldrich syndrome' protein. *Nature* **399**, 379-383.

Abmayr, S. M. and Pavlath, G. K. (2012). Myoblast fusion: lessons from flies and mice. *Development* **139**, 641-656.

Babushok, D. V., Ostertag, E. M. and Kazazian, H. H., Jr (2007). Current topics in genome evolution: molecular mechanisms of new gene formation. *Cell. Mol. Life Sci.* **64**, 542-554.

Journal of Cell Science

Bataillé, L., Delon, I., Da Ponte, J.P., Brown, N.H. and Jagla, K. (2010). Downstream of identity genes: muscle-type-specific regulation of the fusion process. *Dev. Cell* **19**, 317-328.
Bate, M. (1993). The mesoderm and its derivatives. In *The Development of Drosophila melanogaster* (ed. M. Bate and A. Martinez Ariazs), pp. 1013-1090. Cold Spring Harbor Laboratory Press.
Ben-Yaacov, S., Le Borgne, R., Abramson, I., Schweisguth, F. and Schejter, E. D. (2001). Wasp, the Drosophila Wiskott-Aldrich syndrome gene homologue, is required for cell fate decisions mediated by Notch signaling. *J. Cell Biol.* **152**, 1-14.
Berger, S., Schafer, G., Kesper, D. A., Holz, A., Eriksson, T., Palmer, R. H., Beck, L., Klambt, C., Renkawitz-Pohl, R. and Onel, S.-F. (2008). WASP and SCAR have distinct roles in activating the Arp2/3 complex during myoblast fusion. *J. Cell Sci.* **121**, 1303-1313.
Bogdan, S. and Klämbt, C. (2003). Kette regulates actin dynamics and genetically interacts with Wave and Wasp. *Development* **130**, 4427-4437.
Bogdan, S., Grewe, O., Strunk, M., Mertens, A. and Klämbt, C. (2004). Sra-1 interacts with Kette and Wasp and is required for neuronal and bristle development in Drosophila. *Development* **131**, 3981-3989.
Bogdan, S., Stephan, R., Lobke, C., Mertens, A. and Klämbt, C. (2005). Abi activates WASP to promote sensory organ development. *Nat. Cell Biol.* **7**, 977-984.
Brand, A. H. and Perrimon, N. (1993). Targeted gene expression as a means of altering cell fates and generating dominant phenotypes. *Development* **118**, 401-415.
Breitsprecher, D., Kiesewetter, A. K., Linkner, J., Urbanke, C., Resch, G. P., Small, J. V. and Faix, J. (2008). Clustering of VASP actively drives processive, WH2 domain-mediated actin filament elongation. *EMBO J.* **27**, 2943-2954.
Breitsprecher, D., Kiesewetter, A. K., Linkner, J., Vinzenz, M., Stradal, T. E. B., Small, J. V., Curth, U., Dickinson, R. B. and Faix, J. (2011). Molecular mechanism of Ena/VASP-mediated actin-filament elongation. *EMBO J.* **30**, 456-467.
Buljan, M. and Bateman, A. (2009). The evolution of protein domain families. *Biochem. Soc. Trans.* **37**, 751-755.
Buttgereit, D., Paululat, A. and Renkawitz-Pohl, R. (1996). Muscle development and attachment to the epidermis is accompanied by expression of beta 3 and beta1 tubulin isotypes, respectively. *Int. J. Dev. Biol.* **40**, 189-196.
Campellone, K. G. and Welch, M. D. (2010). A nucleator arms race: cellular control of actin assembly. *Nat. Rev. Mol. Cell Biol.* **11**, 237-251.
Campellone, K. G., Webb, N. J., Znameroski, E. A. and Welch, M. D. (2008). WHAMM is an Arp2/3 complex activator that binds microtubules and functions in ER to Golgi transport. *Cell* **134**, 148-161.
Carmena, A., Bate, M. and Jiménez, F. (1995). lethal of scute, a proneural gene, participates in the specification of muscle progenitors during Drosophila embryogenesis. *Genes Dev.* **9**, 2373-2383.
Chen, Z., Borek, D., Padrick, S. B., Gomez, T. S., Metlagel, Z., Ismail, A. M., Umetani, J., Billadeau, D. D., Otwinowski, Z. and Rosen, M. K. (2010). Structure and control of the actin regulatory WAVE complex. *Nature* **468**, 533-538.
Chen, X. J., Squarr, A. J., Stephan, R., Chen, B., Higgins, T. E., Barry, D. J., Martin, M. C., Rosen, M. K., Bogdan, S. and Way, M. (2014). Ena/VASP proteins cooperate with the WAVE complex to regulate the actin cytoskeleton. *Dev. Cell* **30**, 569-584.
Claverie, J.-M. (2001). Gene number: what if there are only 30,000 human genes? *Science* **291**, 1255-1257.
Deng, S., Bothe, I. and Baylies, M. K. (2015). The Formin Diaphanous Regulates Myoblast Fusion through Actin Polymerization and Arp2/3 Regulation. *PLoS Genet.* **11**, e1005381.
Derry, J. M., Ochs, H. D. and Francke, U. (1994). Isolation of a novel gene mutated in Wiskott-Aldrich syndrome. *Cell* **78**, 635-644.
Dhanyasi, N., Segal, D., Shimoni, E., Shinder, V., Shilo, B.-Z., VijayRaghavan, K. and Schejter, E. D. (2015). Surface apposition and multiple cell contacts promote myoblast fusion in Drosophila flight muscles. *J. Cell Biol.* **211**, 191-203.
Eden, S., Rohatgi, R., Podtelejnikov, A. V., Mann, M. and Kirschner, M. W. (2002). Mechanism of regulation of WAVE1-induced actin nucleation by Rac1 and Nck. *Nature* **418**, 790-793.
Fricke, R., Gohl, C., Dharmalingam, E., Grevelhorster, A., Zahedi, B., Harden, N., Kessels, M., Qualmann, B. and Bogdan, S. (2009). Drosophila Cip4/Toca-1 integrates membrane trafficking and actin dynamics through WASP and SCAR/WAVE. *Curr. Biol.* **19**, 1429-1437.
Gho, M., Bellaiche, Y. and Schweisguth, F. (1999). Revisiting the Drosophila microchaete lineage: a novel intrinsically asymmetric cell division generates a glial cell. *Development* **126**, 3573-3584.
Gildor, B., Massarwa, R., Shilo, B.-Z. and Schejter, E. D. (2009). The SCAR and WASp nucleation-promoting factors act sequentially to mediate Drosophila myoblast fusion. *EMBO Rep.* **10**, 1043-1050.
Hansen, S. D. and Mullins, R. D. (2010). VASP is a processive actin polymerase that requires monomeric actin for barbed end association. *J. Cell Biol.* **191**, 571-584.
Junemann, A., Winterhoff, M., Nordholz, B., Rottner, K., Eichinger, L., Gräf, R. and Faix, J. (2013). ForC lacks canonical formin activity but bundles actin filaments and is required for multicellular development of Dictyostelium cells. *Eur. J. Cell Biol.* **92**, 201-212.
Kaipa, B. R., Shao, H., Schafer, G., Trinkewitz, T., Groth, V., Liu, J., Beck, L., Bogdan, S., Abmayr, S. M. and Onel, S.-F. (2013). Dock mediates Scar- and WASp-dependent actin polymerization through interaction with cell adhesion molecules in founder cells and fusion-competent myoblasts. *J. Cell Sci.* **126**, 360-372.
Kesper, D. A., Stute, C., Buttgereit, D., Kreiskother, N., Vishnu, S., Fischbach, K.-F. and Renkawitz-Pohl, R. (2007). Myoblast fusion in *Drosophila melanogaster* is mediated through a fusion-restricted myogenic-adhesive structure (FuRMAS). *Dev. Dyn.* **236**, 404-415.
Kollmar, M., Lbik, D. and Enge, S. (2012). Evolution of the eukaryotic ARP2/3 activators of the WASP family: WASP, WAVE, WASH, and WHAMM, and the proposed new family members WAWH and WAML. *BMC Res. Notes* **5**, 88.
Kovar, D. R., Harris, E. S., Mahaffy, R., Higgs, H. N. and Pollard, T. D. (2006). Control of the assembly of ATP- and ADP-actin by formins and profilin. *Cell* **124**, 423-435.
Krause, M. and Gautreau, A. (2014). Steering cell migration: lamellipodium dynamics and the regulation of directional persistence. *Nat. Rev. Mol. Cell Biol.* **15**, 577-590.
Kumar, V., Fricke, R., Bhar, D., Reddy-Alla, S., Krishnan, K. S., Bogdan, S. and Ramaswami, M. (2009). Syndapin promotes formation of a postsynaptic membrane system in Drosophila. *Mol. Biol. Cell.* **20**, 2254-2264.
Lammel, U., Bechtold, M., Risse, B., Berh, D., Fleige, A., Bunse, I., Jiang, X., Klämbt, C. and Bogdan, S. (2014). The Drosophila FHOD1-like formin Knittrig acts through Rok to promote stress fiber formation and directed macrophage migration during the cellular immune response. *Development* **141**, 1366-1380.
Leibfried, A., Fricke, R., Morgan, M. J., Bogdan, S. and Bellaiche, Y. (2008). Drosophila Cip4 and WASp define a branch of the Cdc42-Par6-aPKC pathway regulating E-cadherin endocytosis. *Curr. Biol.* **18**, 1639-1648.
Linardopoulou, E. V., Parghi, S. S., Friedman, C., Osborn, G. E., Parkhurst, S. M. and Trask, B. J. (2007). Human subtelomeric WASH genes encode a new subclass of the WASP family. *PLoS Genet.* **3**, e237.
Loisel, T. P., Boujemaa, R., Pantaloni, D. and Carlier, M. F. (1999). Reconstitution of actin-based motility of Listeria and Shigella using pure proteins. *Nature* **401**, 613-616.
Lynch, M. and Conery, J. S. (2000). The evolutionary fate and consequences of duplicate genes. *Science* **290**, 1151-1155.
Massarwa, R., Carmon, S., Shilo, B.-Z. and Schejter, E. D. (2007). WIP/WASp-based actin-polymerization machinery is essential for myoblast fusion in Drosophila. *Dev. Cell* **12**, 557-569.
Miki, H., Miura, K. and Takenawa, T. (1996). N-WASP, a novel actin-depolymerizing protein, regulates the cortical cytoskeletal rearrangement in a PIP2-dependent manner downstream of tyrosine kinases. *EMBO J.* **15**, 5326-5335.
Miki, H., Suetsugu, S. and Takenawa, T. (1998). WAVE, a novel WASP-family protein involved in actin reorganization induced by Rac. *EMBO J.* **17**, 6932-6941.
Moreira, C. G. A., Jacinto, A. and Prag, S. (2013). Drosophila integrin adhesion complexes are essential for hemocyte migration in vivo. *Biol. Open* **2**, 795-801.
Mukherjee, P., Gildor, B., Shilo, B.-Z., VijayRaghavan, K. and Schejter, E. D. (2011). The actin nucleator WASp is required for myoblast fusion during adult Drosophila myogenesis. *Development* **138**, 2347-2357.
Nose, A., Isshiki, T. and Takeichi, M. (1998). Regional specification of muscle progenitors in Drosophila: the role of the msh homeobox gene. *Development* **125**, 215-223.
Pollard, T. D. (2007). Regulation of actin filament assembly by Arp2/3 complex and formins. *Annu. Rev. Biophys. Biomol. Struct.* **36**, 451-477.
Pollard, T. D. and Beltzner, C. C. (2002). Structure and function of the Arp2/3 complex. *Curr. Opin. Struct. Biol.* **12**, 768-774.
Pollitt, A. Y. and Insall, R. H. (2009). WASP and SCAR/WAVE proteins: the drivers of actin assembly. *J. Cell Sci.* **122**, 2575-2578.
Rajan, A., Tien, A.-C., Haueter, C. M., Schulze, K. L. and Bellen, H. J. (2009). The Arp2/3 complex and WASp are required for apical trafficking of Delta into microvilli during cell fate specification of sensory organ precursors. *Nat. Cell Biol.* **11**, 815-824.
Richardson, B. E., Beckett, K., Nowak, S. J. and Baylies, M. K. (2007). SCAR/WAVE and Arp2/3 are crucial for cytoskeletal remodeling at the site of myoblast fusion. *Development* **134**, 4357-4367.
Rohatgi, R., Ma, L., Miki, H., Lopez, M., Kirchhausen, T., Takenawa, T. and Kirschner, M. W. (1999). The interaction between N-WASP and the Arp2/3 complex links Cdc42-dependent signals to actin assembly. *Cell* **97**, 221-231.
Rotkopf, S., Hamberg, Y., Aigaki, T., Snapper, S. B., Shilo, B.-Z. and Schejter, E. D. (2011). The WASp-based actin polymerization machinery is required in somatic support cells for spermatid maturation and release. *Development* **138**, 2729-2739.

Rottner, K. and Stradal, T. E. B. (2011). Actin dynamics and turnover in cell motility. *Curr. Opin. Cell Biol.* **23**, 569-578.
Ruiz-Gomez, M., Coutts, N., Price, A., Taylor, M. V. and Bate, M. (2000). Drosophila Dumbfounded: a myoblast attractant essential for fusion. *Cell* **102**, 189-198.
Sander, M., Squarr, A. J., Risse, B., Jiang, X. and Bogdan, S. (2013). Drosophila pupal macrophages–a versatile tool for combined ex vivo and in vivo imaging of actin dynamics at high resolution. *Eur. J. Cell Biol.* **92**, 349-354.
Schafer, G., Weber, S., Holz, A., Bogdan, S., Schumacher, S., Muller, A., Renkawitz-Pohl, R. and Onel, S.-F. (2007). The Wiskott-Aldrich syndrome protein (WASP) is essential for myoblast fusion in Drosophila. *Dev. Biol.* **304**, 664-674.
Sens, K. L., Zhang, S., Jin, P., Duan, R., Zhang, G., Luo, F., Parachini, L. and Chen, E. H. (2010). An invasive podosome-like structure promotes fusion pore formation during myoblast fusion. *J. Cell Biol.* **191**, 1013-1027.
Spudich, J. A. and Watt, S. (1971). The regulation of rabbit skeletal muscle contraction. I. Biochemical studies of the interaction of the tropomyosin-troponin complex with actin and the proteolytic fragments of myosin. *J. Biol. Chem.* **246**, 4866-4871.
Stephan, R., Gohl, C., Fleige, A., Klämbt, C. and Bogdan, S. (2011). Membrane-targeted WAVE mediates photoreceptor axon targeting in the absence of the WAVE complex in Drosophila. *Mol. Biol. Cell* **22**, 4079-4092.
Stradal, T. E. B. and Scita, G. (2006). Protein complexes regulating Arp2/3-mediated actin assembly. *Curr. Opin. Cell Biol.* **18**, 4-10.
Suarez, C., Carroll, R. T., Burke, T. A., Christensen, J. R., Bestul, A. J., Sees, J. A., James, M. L., Sirotkin, V. and Kovar, D. R. (2015). Profilin regulates F-actin network homeostasis by favoring formin over Arp2/3 complex. *Dev. Cell* **32**, 43-53.
Suetsugu, S., Yamazaki, D., Kurisu, S. and Takenawa, T. (2003). Differential roles of WAVE1 and WAVE2 in dorsal and peripheral ruffle formation for fibroblast cell migration. *Dev. Cell* **5**, 595-609.
Takenawa, T. and Suetsugu, S. (2007). The WASP-WAVE protein network: connecting the membrane to the cytoskeleton. *Nat. Rev. Mol. Cell Biol.* **8**, 37-48.
Tal, T., Vaizel-Ohayon, D. and Schejter, E. D. (2002). Conserved interactions with cytoskeletal but not signaling elements are an essential aspect of Drosophila WASp function. *Dev. Biol.* **243**, 260-271.
Veltman, D. M. and Insall, R. H. (2010). WASP family proteins: their evolution and its physiological implications. *Mol. Biol. Cell* **21**, 2880-2893.
Yan, S., Lv, Z., Winterhoff, M., Wenzl, C., Zobel, T., Faix, J., Bogdan, S. and Grosshans, J. (2013). The F-BAR protein Cip4/Toca-1 antagonizes the formin Diaphanous in membrane stabilization and compartmentalization. *J. Cell Sci.* **126**, 1796-1805.
Yang, Z. (2007). PAML 4: phylogenetic analysis by maximum likelihood. *Mol. Biol. Evol.* **24**, 1586-1591.
Yang, Z. (1998). Likelihood ratio tests for detecting positive selection and application to primate lysozyme evolution. *Mol. Biol. Evol.* **15**, 568-573.
Zallen, J. A., Cohen, Y., Hudson, A. M., Cooley, L., Wieschaus, E. and Schejter, E. D. (2002). SCAR is a primary regulator of Arp2/3-dependent morphological events in Drosophila. *J. Cell Biol.* **156**, 689-701.
Zobel, T. and Bogdan, S. (2013). A high resolution view of the fly actin cytoskeleton lacking a functional WAVE complex. *J. Microsc.* **251**, 224-231.
Zobel, T., Brinkmann, K., Koch, N., Schneider, K., Seemann, E., Fleige, A., Qualmann, B., Kessels, M. M. and Bogdan, S. (2015). Cooperative functions of the two F-BAR proteins Cip4 and Nostrin in the regulation of E-cadherin in epithelial morphogenesis. *J. Cell Sci.* **128**, 499-515.
Zuchero, J. B., Coutts, A. S., Quinlan, M. E., Thangue, N. B. L. and Mullins, R. D. (2009). p53-cofactor JMY is a multifunctional actin nucleation factor. *Nat. Cell Biol.* **11**, 451-459.

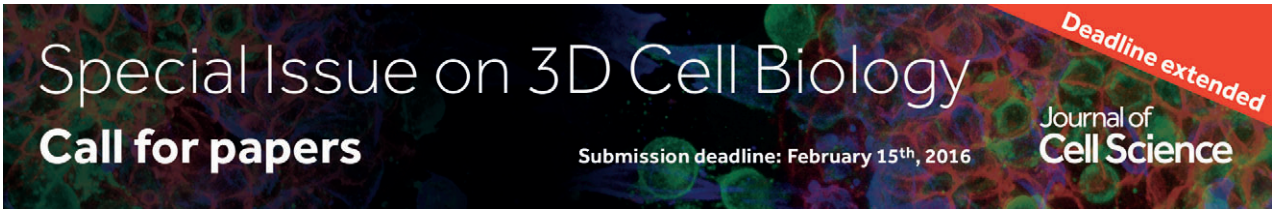

Journal of Cell Science